AD-A090 021 TUFTS UNIV MEDFORD MASS DEPT OF PHYSICS F/G 3/2
FINE-SCALE RADIO STUDIES OF THE SUN.(U)
JUL 80 K R LANG, R F WILLSON F19628-79-C-0010
UNCLASSIFIED AFGL-TR-80-0190 NL

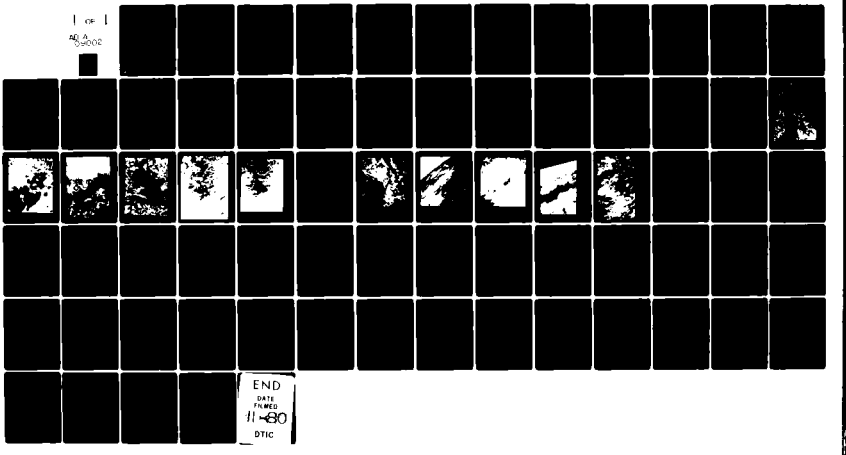

LEVEL II

12

AFGL-TR-80-0190

AD A090021

FINE-SCALE RADIO STUDIES OF THE SUN

Kenneth R. Lang
Robert F. Willson

Department of Physics
Tufts University
Medford, MA 02155

1 July 1980

FINAL SCIENTIFIC REPORT
15 December 1978 to 15 June 1980

Approved for public release; distribution unlimited.

AIR FORCE GEOPHYSICS LABORATORY
AIR FORCE SYSTEMS COMMAND
UNITED STATE AIR FORCE
HANSCOM AFB, MASSACHUSETTS 01731

SECURITY CLASSIFICATION OF THIS PAGE (When Data Entered)

REPORT DOCUMENTATION PAGE

READ INSTRUCTIONS BEFORE COMPLETING FORM

1. REPORT NUMBER: AFGL-TR-80-0190	2. GOVT ACCESSION NO.: AD-A090 027
3. RECIPIENT'S CATALOG NUMBER:	
4. TITLE (and Subtitle): Fine-Scale Radio Studies of the Sun	5. TYPE OF REPORT & PERIOD COVERED: Final Scientific Report, 15 Dec. 1978 - 15 June 1980
	6. PERFORMING ORG. REPORT NUMBER:
7. AUTHOR(s): Kenneth R. Lang and Robert F. Willson	8. CONTRACT OR GRANT NUMBER(s): F 19628-79-C-0010
9. PERFORMING ORGANIZATION NAME AND ADDRESS: Department of Physics, Tufts University, Medford, MA 02155	10. PROGRAM ELEMENT, PROJECT, TASK AREA & WORK UNIT NUMBERS: 61102F 2311G3 BD
11. CONTROLLING OFFICE NAME AND ADDRESS: Air Force Geophysics Laboratory, Hanscom AFB, Massachusetts 01731, Contract Monitor: Donald Guidice/PHP	12. REPORT DATE: 1 July 1980
	13. NUMBER OF PAGES: 71
14. MONITORING AGENCY NAME & ADDRESS (if different from Controlling Office)	15. SECURITY CLASS (of this report): Unclassified
	15a. DECLASSIFICATION DOWNGRADING SCHEDULE:

16. DISTRIBUTION STATEMENT (of this Report)

Approved for public release, distribution unlimited.

17. DISTRIBUTION STATEMENT (of the abstract entered in Block 20, if different from Report)

18. SUPPLEMENTARY NOTES

19. KEY WORDS (Continue on reverse side if necessary and identify by block number)

Solar Radio Radiation, Very Large Array, Solar Corona, Active Regions, Magnetic Field, Polarization, Temperature, Bremsstrahlung, Electron Density, Plage.

20. ABSTRACT (Continue on reverse side if necessary and identify by block number)

Very Large Array (V.L.A.) synthesis maps at 6 cm wavelength are presented for six different active regions on seven different days scattered over a one and a half year period. In every case the active region has been resolved into one or more small ($\leq 20''$), bright ($\geq 10^6$ K) highly circularly polarized (30% to 100%) sources which dominate active region emission at 6 cm wavelength. Although each small bright source and each active region has one dominant magnetic polarity, several active regions contained a few small bright sources

DD FORM 1 JAN 73 1473 EDITION OF 1 NOV 65 IS OBSOLETE

SECURITY CLASSIFICATION OF THIS PAGE (When Data Entered)

20.(cont.)

with opposite senses of circular polarization. Comparisons of the synthesis maps of total intensity with Hα photographs of the same active regions indicate that the enhanced 6 cm emission is well correlated with the chromospheric plage seen as bright regions on the Hα photographs, and that there is often no similar enhanced 6 cm emission in the regions which directly overly sunspots. The large brightness temperatures of the regions of enhanced 6 cm emission indicate an origin in the coronal atmosphere above active regions whereas comparisons of the synthesis maps of circular polarization with magnetograms of the underlying photosphere indicate that these maps act as coronal magnetograms. The maps of circular polarization exhibit magnetic polarities, dipole shapes, orientations and extents which are similar to those found by the Zeeman effect in the photosphere. Both the circular polarization maps and the Zeeman effect magnetograms refer to the longitudinal component of the magnetic field, and the regions of enhanced 6 cm emission are well correlated with this component. We interpret the enhanced 6 cm emission in terms of the thermal bremsstrahlung of a hot (electron temperature $T_e \approx 2.5 \times 10^6$ K), dense (emission measure $\int N_e^2 \, dl \approx 2 \times 10^{29}$ cm^{-5} and electron density $N_e \approx 5 \times 10^9$ cm^{-3}) "coronal condensations" which overly bright chromospheric plage. The spatial configuration, emission measure, electron density and temperature are all consistent with those inferred from X-ray observations of the coronal atmosphere above other active regions. Magnetic field strengths of between 450 and 900 Gauss are required at levels where the temperature exceeds a million degrees if the observed circular polarization is explained by either thermal bremsstrahlung or gyroresonance absorption. We propose a multiple component model in which the slowly varying component of solar radio radiation is predominantly due to the thermal bremsstrahlung of a variety of sources with angular sizes ranging from 10" to 10' and brightness temperatures and electron densities which decrease with increasing size. Our model does not exclude the possibility that gyroresonant absorption processes can become important near sunspots under special conditions, but these processes do not dominate the 6 cm emission from the active regions which we have observed.

We also present observations of solar flares using the Owens Valley interferometer at 2.8 wavelength. These observations were made for the purpose of studying changes in the circular polarization which have previously been seen minutes before flares occur. The changes in circular polarization are thought to be due to emerging magnetic fields which may forcast flare eruption before their actual occurrence. During a two week observing session, 14 flares of weak to moderate (1 to 10 solar flux units) were detected. No impulsive polarization changes were seen before any of the flares but a few gradual changes were detected before, during and after some events which might be caused by gradual reconfigurations of the coronal magnetic fields.

TABLE OF CONTENTS

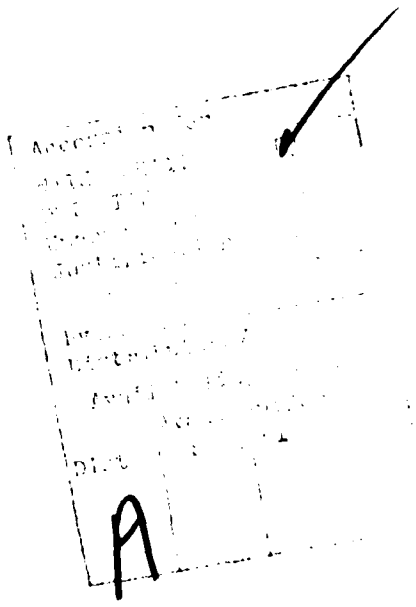

A. INTRODUCTION

It has long been known that the slowly varying (S) component of solar radio emission, whose intensity is correlated with sunspot number and area, is connected with solar activity and has its origin in solar active regions. Previous interpretations of the emission mechanism and correlations with features seen at optical wavelengths have been limited by the low angular resolutions available at the time, however, for the large antenna beam-widths artificially dilute estimates of polarization and brightness, and they do not usually discriminate between groups of sunspots and the hot plasma located between them. The two prevailing hypotheses for the emission mechanism of the S component are the thermal bremsstrahlung of hot and dense (electron temperature $T_e \sim 2 \times 10^6$ K and electron density $N_e \sim 10^9$ to 10^{10} cm^{-3}) "coronal condensations" (Waldemeier and Müller, 1950; Waldemeier, 1956; Christiansen and Mathewson, 1959; Christiansen et al., 1960; Newkirk, 1961) and the magneto-bremsstrahlung involing gyroresonance absorption in the intense magnetic fields of sunspots (Stepanov, 1958; Ginzburg and Zheleznyakov, 1959; Zheleznyakov, 1962; Lantos, 1968; Zlotnik 1968 a, b, and Zheleznyakov 1970). When gyroresonant absorption has been invoked, it has usually been related to the so-called core-halo model which is based upon Kundu's (1959a, b) interferometric observations which showed that the S component sources at 3.2 cm contain an intense polarized ($\sim$ 30%) core with an angular size $\theta \lesssim 1.8'$ surrounded by a weaker unpolarized halo whose angular extent ranges between 5' and 9'. According to the core-halo model, the intense polarized cores are related to gyro-magnetic processes in the magnetic fields of sunspots, whereas the extended,

unpolarized halo emission is associated with the thermal bremsstrahlung of chromospheric plage. It soon became apparent, however, that the observations which have been used in support of these models could have led to misleading conclusions, for the unresolved "cores" could be associated with either sunspots or bright plage, the polarization measurements could be affected by beam dilution effects, and the observed circular polarization could be accounted for by propagation effects without an appeal to gyroresonant absorption (Covington, 1949; Lehany and Yabsley, 1949; Denisse, 1950; Gelfreich et al., 1959).

By the 1970's the development of high resolution radio wavelength interferometers and synthesis arrays led to a renewed interest in the competing models for the structure of the coronal atmosphere above solar active regions. Lang (1974 a) for example, used interferometric observations at a wavelength of $\lambda = 3.7$ cm with an effective angular resolution of 7" to show that the so-called core sources are actually composed of one or more sources with angular sizes of $\theta \sim 20"$, brightness temperatures of $T_B \sim 10^6$ K, and extraordinarily high circular polarizations of up to 100%. The presence of several bright core components with angular sizes of about 20" and brightness temperatures ranging between 5×10^5 and 10^7 K was confirmed by interferometric observations of 2.8 cm wavelength (Felli, Pampaloni and Tofani, 1974; Felli, Tofani, Fürst and Hirth, 1975). Kundu and Alissandrakis (1975) next used the Westerbork Synthesis Radio Telescope (W.S.R.T.) at a wavelength of $\lambda = 6$ cm to resolve a solar active region into several discrete sources with brightness temperatures of $T_B \gtrsim 10^6$ K. They were able to show that the circular polarization of these smaller sources is as high as 90%, and that maps of the circular polarization

correlate well with magnetograms of the longitudinal magnetic field in the lower lying solar photosphere. Subsequent analysis of the data by Kundu, Alissandrakis, Bregman and Hin (1977) suggested that the brightest components of the 6 cm emission are associated with sunspots, but some of the brightest sources were actually associated with chromospheric plage where no sunspots exist.

In this report we present Very Large Array (V.L.A.) observations at 6 cm wavelength for six different active regions on seven different days scattered over a one and a half year period. Although many of the earlier observations were made when the V.L.A. was in the early stages of construction, the effective angular resolution of $\tilde{>}$ 10" for these pioneering observations was sufficient to resolve the dominant sources of enhanced emission and to show that they are predominantly associated with the bright chromospheric plage. In fact, now that the full V.L.A. is available, the detailed morphological features and structural changes of the 6 cm emission can be compared with similar features and changes in the bright plage with second-of-arc accuracy (Felli, Lang and Willson, 1980). The earlier observations presented here provide a fairly large sample spread over a long period of time, and allow us to make several definitive conclusions in spite of the fact that the full potential of the V.L.A. was not always available. The synthesis maps given in Section B , for example, indicate that in every case the observed active region has been resolved into one or more small ($\tilde{<}$ 20"), bright ($\tilde{>}$ 10^6K), highly circularly polarized (30% to 100%) sources which dominate active region emission at 6 cm wavelength. Here we also show that the enhanced emission coincides in shape, orientation and extent with the chromospheric

plage which is seen as bright regions on H α photographs, and that there is often no similar enhanced 6 cm emission in the regions which directly overly sunspots. The large brightness temperatures of $\sim 10^6$K indicate an origin in the coronal atmosphere above active regions, and our results are consistent with recent X-ray and E.U.V. observations which indicate that a hot dense coronal plasma is located in magnetic arches between sunspots, and that cooler tenuous regions overly sunspots. In Section II we also show that the circular polarization at 6 cm wavelength exhibits magnetic polarities, dipole shapes, orientations and extents which are correlated with the structure of the longitudinal magnetic field seen in magnetograms of the lower lying photosphere. A connection between regions of enhanced radio emission and the surface magnetic field of the Sun has been suggested by Tanaka and Steinberg (1964), Kundu and McCullough (1972), Felli, Poletto and Tofani (1977), Kundu, Alissandrakis, Bregman and Hin (1977) and Chiuderi Drago, Felli and Tofani (1977); and here we expand upon Lang and Willson's (1979, 1980) contention that the 6 cm maps of circular polarization delineate the magnetic structure in coronal regions where the temperatures exceed a million degrees.

Another aspect of our work, more directly related to the prediction of solar flares, was the monitoring of the circular polarization of active regions. The purpose of these observations was to identify any polarization changes which occur before flares and which may therefore serve as warnings for the commencement of flare activity. In Section C we present these observations at 2.8 cm wavelength at the Owens Valley Observatory during a two week period in December 1979. Fourteen flares of weak to moderate intensity were detected and none exhibited rapid polarization changes minutes or hours before the events. In a few cases however, gradual polarization

changes were seen.

In Section D a theoretical discussion is provided in which the several observed regions of the sources described in Section II are interpreted in terms of the thermal bremsstrahlung process. The fact that the peak brightness temperature of each source always lies in the range 2 to 4 x 10^6 K, suggests that the brightest features of the enhanced radio emission have become optically thick with a brightness temperature equal to the electron temperature in the coronal atmosphere; wheras the larger part of the enhanced emission comes from optically thin coronal regions. By using a representative optical depth of $\tau = 0.3$ and a representative electrontemperature of $T_e = 2.5 \times 10^6$ K, the thermal bremsstrahlung formulae indicate an emission measure of $\int N_e^2 dl \approx 2 \times 10^{29}$ cm^{-5} and an average electron density of $N_e \approx 5 \times 10^9$ cm^{-3}. These physical parameters are consistent with those inferred from X-ray observations of the coronal atmosphere above solar active regions. We therefore revive the old "coronal condensation" hypothesis for the slowly varying component of radio emission, and argue that an appeal to gyroresonant absorption is not needed, at least for the 6 cm observations presented here. Instead, our observations indicate that the previously unresolved cores in the old (Kundu, 1959 a,b) core-halo model may actually be predominantly due to the bremsstrahlung of dense coronal condensations which overly bright plage rather than gyromagnetic emission associated with sunspots. We do not exclude the possibility of gyroresonsnt absorption becoming dominant under very special conditions near sunspots, but our sample of six different active regions indicates that thermal bremsstrahlung from the coronal regions which lie between sunspots dominates the 6 cm radiation from active regions. In Section D we also show that the high degree of circular polarization requires intense magnetic fields of between 450 and 900 Gauss in coronal levels where the temperatures exceed a

million degrees. This conclusion follows from either the thermal bremsstrahlung or the gyroresonant absorption hypothesis, and the observed data indicate that these intense fields exist in regions of bright chromospheric plage which are not necessarily associated with sunspots. Finally in this section, we show that the reversals in sign of the circular polarization which are often observed during solar flares can be explained if the flare heats an overlying layer causing the optical depth in this layer to decrease. In the final Section E, we summarize our basic conclusions.

B. VLA OBSERVATIONAL RESULTS

We have used the Very Large Array (V.L.A.) of the National Radio Astronomy Observatory* to observe six different active regions on seven different days scattered over a one and a half year period. Many of these observations were made with a partially completed array at times when only one arm was available and the Sun was at an unfavorable declination for complete u-v coverage. The effective angular resolutions of $\approx$ 10" for our synthesized beams have enabled us to resolve the dominant sources of enhanced emission, however, and some important general conclusions have been made in spite of some large uncertainties in these pioneering observations. The names of the active regions are given in Table I together with their positions on the Sun's surface, the number of antennae used, the total number of interferometer pairs, and the minimum and maximum interferometer baselines. The individual antennae have a diameter of 25 m which provided a beamwidth of 8.6' and an aperture efficiency of 65% at our operating wavelength of λ = 6 cm. The average correlated flux of each interferometer pair was sampled every 30 s for both the left hand circularly polarized (LCP) and the right hand circularly polarized (RCP) signals. These data were then calibrated, edited and averaged to make synthesis maps of the Stokes parameters I and V.

For each antenna pair the correlator outputs were calibrated by observing 3C 84, CTA 102, or 3C 273 for 5 min every 20 min, whereas the solar active region was observed during the remaining 15 min of each 20 min period. The frequent observations of the calibrator lessened the effects of tropospheric refraction variations, and allowed a calibration of the instrumental gain, polarization and phase according to the

---

*Operated by Associated Universities Inc. under contract with the National Science Foundation.

Table I: Observation date, active region numbers, McMath numbers, positions, reference time, number of antennae, number of interferometer pairs, and the minimum maximum distances from the array center in kilometers for observations of six active regions on seven days.

Date	Active Region	McMath Number	Position Latitude	Position Longitude	At (U.T.)	Antennae	Interferometer Pairs	Baselines Min.	Baselines Max.
3/30/78	1046	15205	$24^{\circ}S$	$7^{\circ}W$	12^{h}	12	50	0.04	11
4/1/78	1056	15220	$12^{\circ}N$	$65^{\circ}E$	0^{h}	12	50	0.04	11
11/4/78	1374	15635	$19^{\circ}S$	$14^{\circ}E$	14^{h}	12	50	0.08	14
11/29/78	1407	15673	$11^{\circ}N$	$48^{\circ}W$	13^{h}	10	45	0.07	11
12/1/78	1429	--	$18^{\circ}S$	$40^{\circ}E$	0^{h}	8	28	0.07	11
10/5/79	2032	--	$17^{\circ}N$	$61^{\circ}E$	13^{h}	10	45	0.04	6
10/6/79	2032	--	$16^{\circ}N$	$45^{\circ}E$	13^{h}	10	45	0.04	6

procedures described by Lang and Willson (1979). For calibration purposes the background temperature of the Sun at 6 cm wavelength was assumed to be 2×10^4 K, and the flux densities of 3C 84, CTA 102 and 3C 273 at $\lambda = 6$ cm were respectively assumed to be 49, 34, and 35 Jy, where 1 Jy = 10^{-23} erg s^{-1} cm^{-2} Hz^{-1} = 10^{26} W m^{-2} Hz^{-1} and one solar flux unit (1 s.f.u.) = 10^4 Jy. The uncertainties in these pioneering observations were larger than those presently available with the V.L.A., for the brightness temperatures reported here are uncertain by a factor of two, and known instrumental effects limit the circular polarization accuracy to about 10%. Nevertheless, the brightness temperatures and circular polarizations are large ($\gtrsim 10^6$ K and up to 100%); and these uncertainties do not preclude important conclusions about the physical parameters of the regions of enhanced radio emission. Solar flares, bad antennae, and interference were edited from the data and the 30 s values of amplitude and phase were then added together to obtain 5 min vector averages with a phase calibration better than 5^o and an amplitude calibration accurate to <10%. These calibrated averages of the amplitude and phase of each polarization for every antenna pair were then taken to be the amplitude and phase of the source visibility function. The source intensity distribution was then obtained by Fourier transforming the visibility function and using the "clean" procedure on nearly 10,000 u-v components for each observation day. Our preliminary results indicated that the data on the longer baselines with angular resolutions $\lesssim$ 10" were contributing noise to our maps, particularly in the early observations when the V.L.A. was still under construction and the Sun was at low declinations where the u-v coverage was poor. We therefore discarded the 6 cm data having fringe spacings $\lesssim$ 10", and used the intensity distributions obtained from the right hand circularly polarized (RCP) and

left hand circularly polarized (LCP) signals to form synthesis maps of the total intensity I = (LCP + RCP)/2 and the circular polarization V = (LCP - RCP)/2. These maps are illustrated in Figures 1 through 7 where the synthesized beam pattern is denoted by a hatched ellipse, the contour intervals are given in units of Jy per synthesized beam area, the I maps contain solid contours only, and the V maps contain solid and dashed contours respectively denoting left-hand circular polarization (positive V) and right hand circular polarization (negative V).

As illustrated in Figures 1 through 7 and Table II, solar active regions always exhibit small ($\lesssim$ 20"), bright ($\lesssim 10^6$ K), highly circularly polarized (30% to 100%) sources which dominate active region emission at 6 cm wavelength. The peak values of brightness temperature T_B given in Table II were determined from the Rayleigh-Jeans law in which $T_B = (S/\Omega_B)\ (\lambda^2/2k)$, the peak flux density is S, the synthesized beam area Ω_B usually took on values of $\lesssim$ 40 square seconds of arc, the observing wavelength is λ = 6 cm, and k is Boltzmann's constant. The peak brightness temperature of each region of enhanced emission usually lies in the range 2 to 4 x 10^6 K, and this suggests that the brightest features have become optically thick with a brightness temperature equal to the electron temperature in the coronal atmosphere [Continuum observations at X-ray wavelengths (Vaiana and Rosner, 1978), as well as the observed Doppler broadening and excitation of spectral lines at optical wavelengths (Newkirk, 1961) indicate that the coronal condensations above active regions have electron temperatures of T_e = 2 to 4 x 10^6 K]. The larger part of the enhanced radio emission is therefore optically thin with a representative optical depth of $\tau = T_B/T_e \lesssim 0.3$ for a representative electron temperature $T_e \lesssim 2.5 \times 10^6$ K. Under this assumption we can compute the emission measures (cf. Equation (1) of

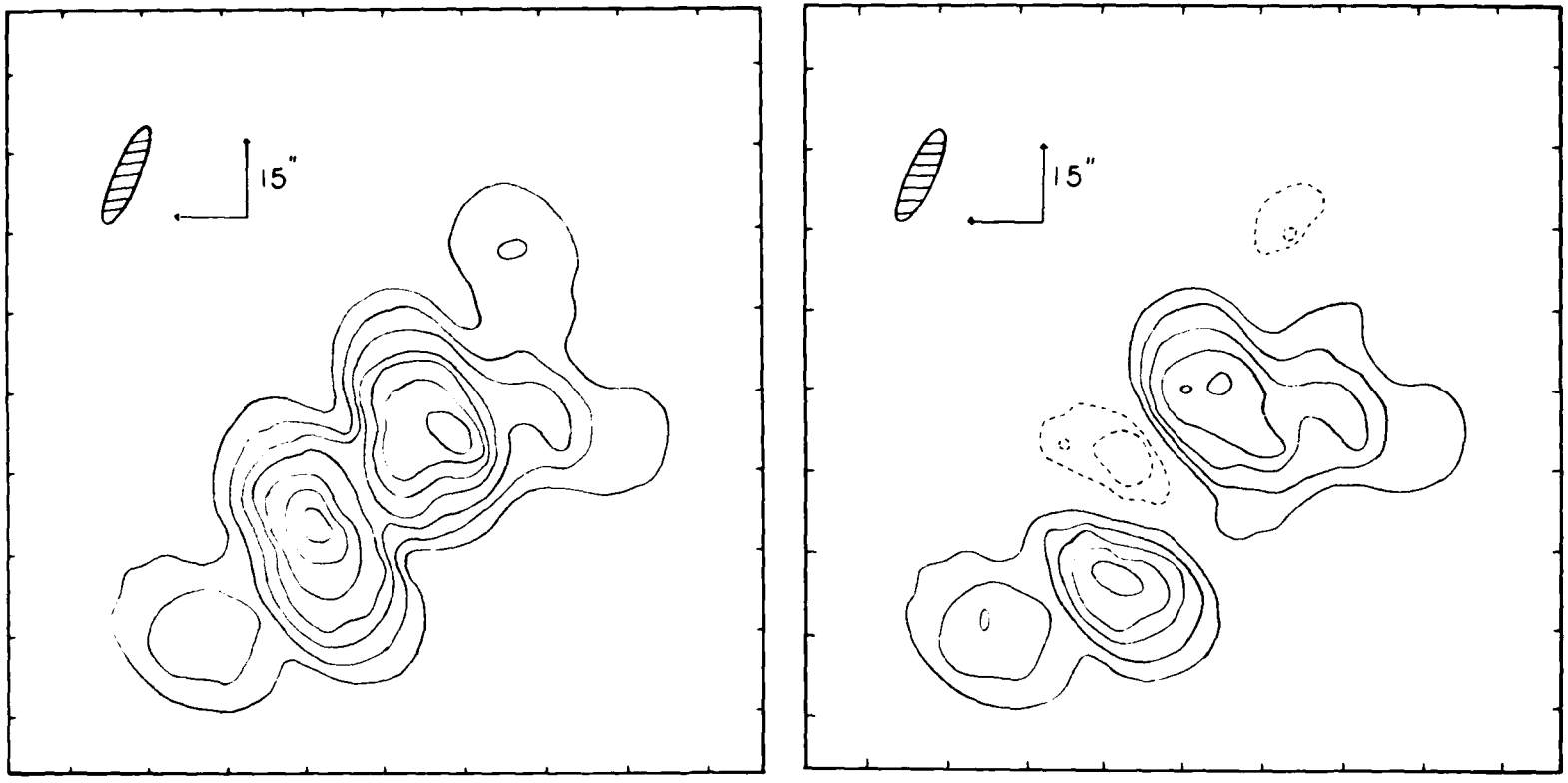

Figure 1. V.L.A. synthesis maps of the total intensity, I (left), and the circular polarization, V (right), at 6 cm wavelength of solar active region AR 1046 (McMath 15205) for one day's observation on March 30, 1978. North is up, East is to the left, dashed lines indicate negative values of V and correspond to right circularly polarized radiation, and solid lines denote positive V values and left circularly polarized radiation. The contours for the I map are at 35, 30, ...5 Jy per square arc second. The maximum positive and negative values of the V contours are +25 and -15 Jy per square arc second, and the contour levels are in steps of 5.

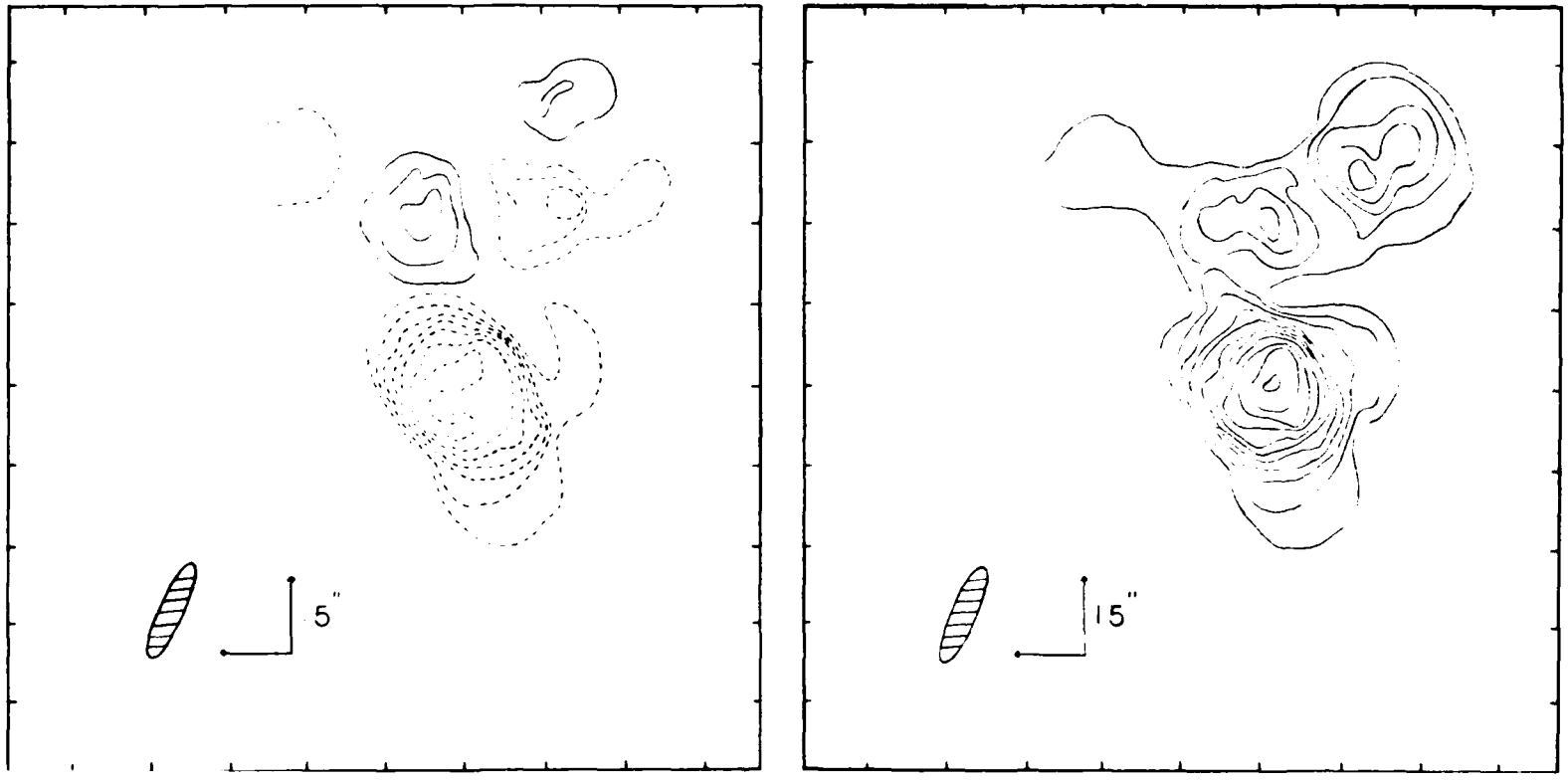

Figure 2. V.L.A. synthesis maps of the total intensity, I (right), and the circular polarization, V (left), at 6 cm wavelength for solar active region AR 1056 (McMath 15220) for one day's observation on April 1, 1978. North is up, East is to the left, dashed lines indicate negative values of V and correspond to right circularly polarized radiation, and solid lines denote positive V values and left circularly polarized radiation. The contours for the I map are at 55, 50, ... 5 Jy per square arc second. The maximum positive and negative values of the V contours are +15 and -40 Jy per square arc second and the contour levels are in steps of 5.

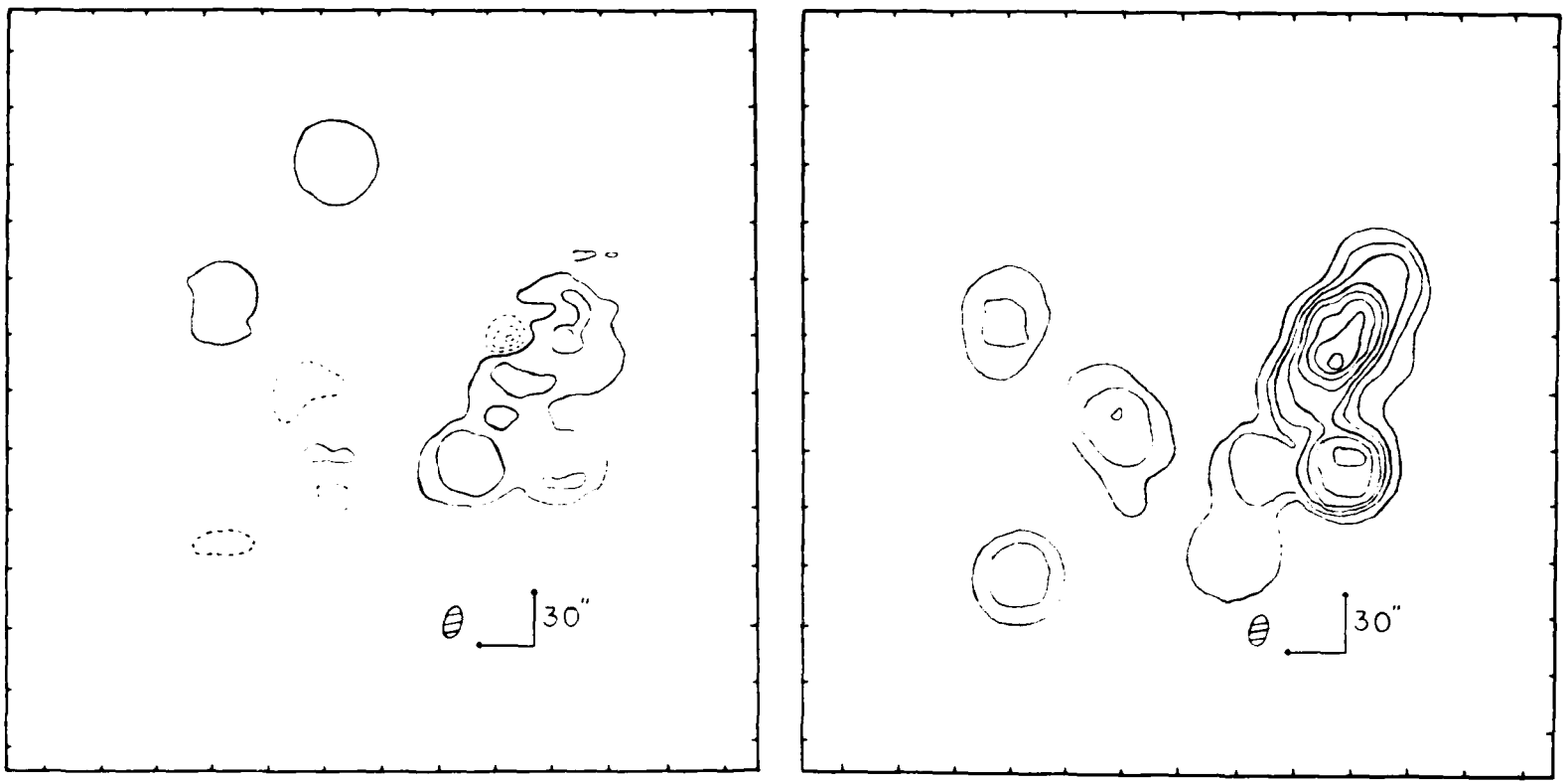

Figure 3. V.L.A. synthesis maps of the total intensity, I (right), and the circular polarization, V (left), at 6 cm wavelength for solar active region AR 1374 (McMath 15635) for one day's observation on November 4, 1978, North is up, East is to the left, dashed lines indicate negative values of V and correspond to right circularly polarized radiation, and solid lines denote positive V values and left circularly polarized radiation. The contours for the I map are at 80, 70 ... 10 Jy per square arc second. The maximum positive and negative values of the V contours are +20 and -30 Jy per square arc second and the contour levels are also in steps of 10.

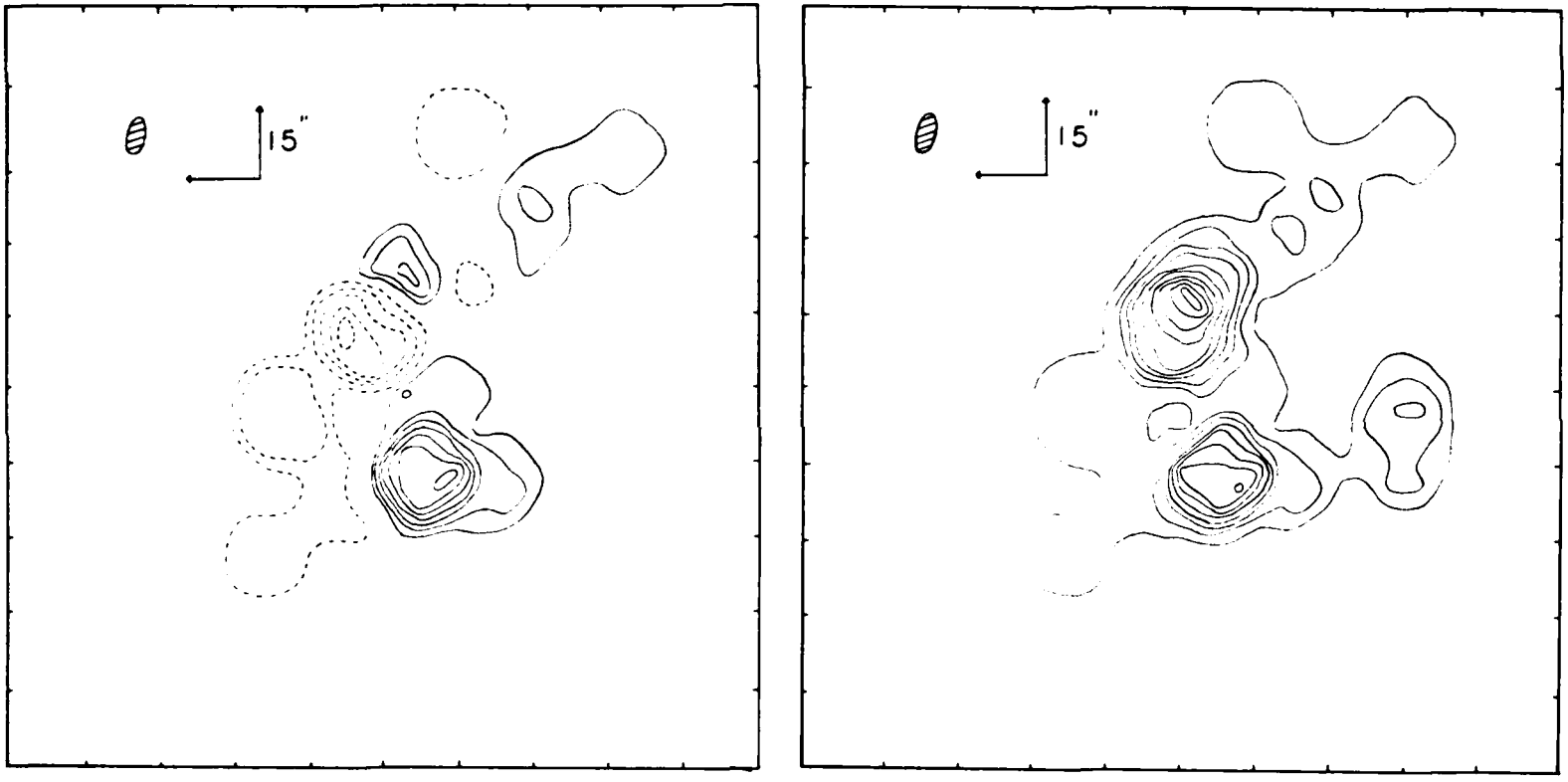

Figure 4. V.L.A. synthesis maps of the total intensity, I (right), and the circular polarization, V (left), at 6 cm wavelength of solar active region AR 1407 (McMath 15673) for one day's observation on November 29, 1978. North is up, East is to the left, dashed lines indicate negative values of V and correspond to right circularly polarized radiation and solid lines denote positive V values and left circularly polarized radiation. The contours for the I map are at 50, 45 ... 5 Jy per square arc second. The maximum positive and negative values of the V contours are +35 and -25 Jy per square arc second, and the contour levels are also in steps of 5.

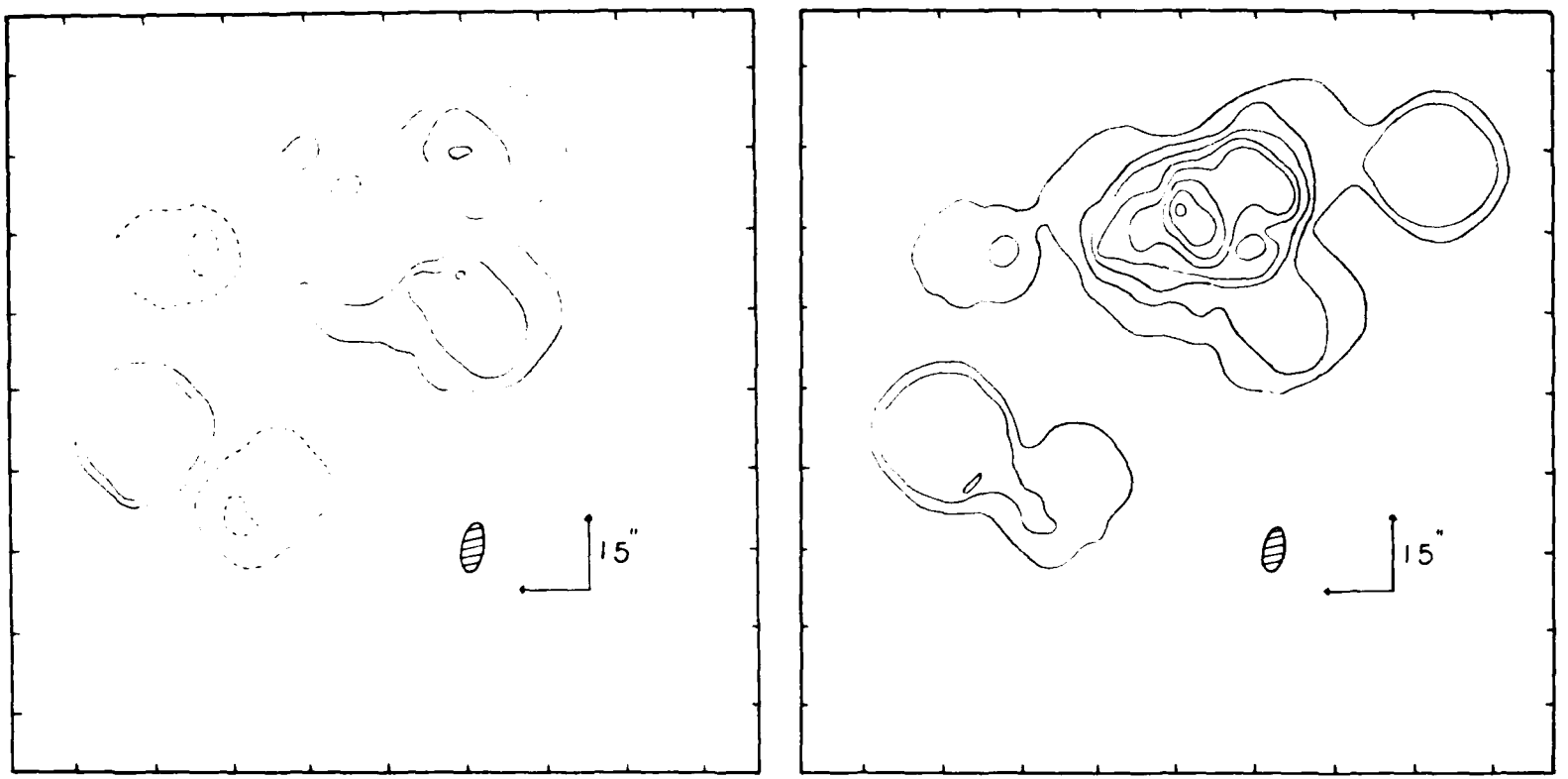

Figure 5. V.L.A. synthesis maps of the total intensity, I (right), and the circular polarization, V (left), at 6 cm wavelength of solar active region AR 1429 for one day's observation on December 1, 1978. North is up, East is to the left, dashed lines indicate negative values of V and correspond to right circularly polarized radiation, and solid lines denote positive V values and left circularly polarized radiation. The contours for the I map are at 200, 175 ... 25 Jy per square arc second. The maximum positive and negative values of the V contours are +75 and -50 Jy per square arc second and the contour levels are also in steps of 25.

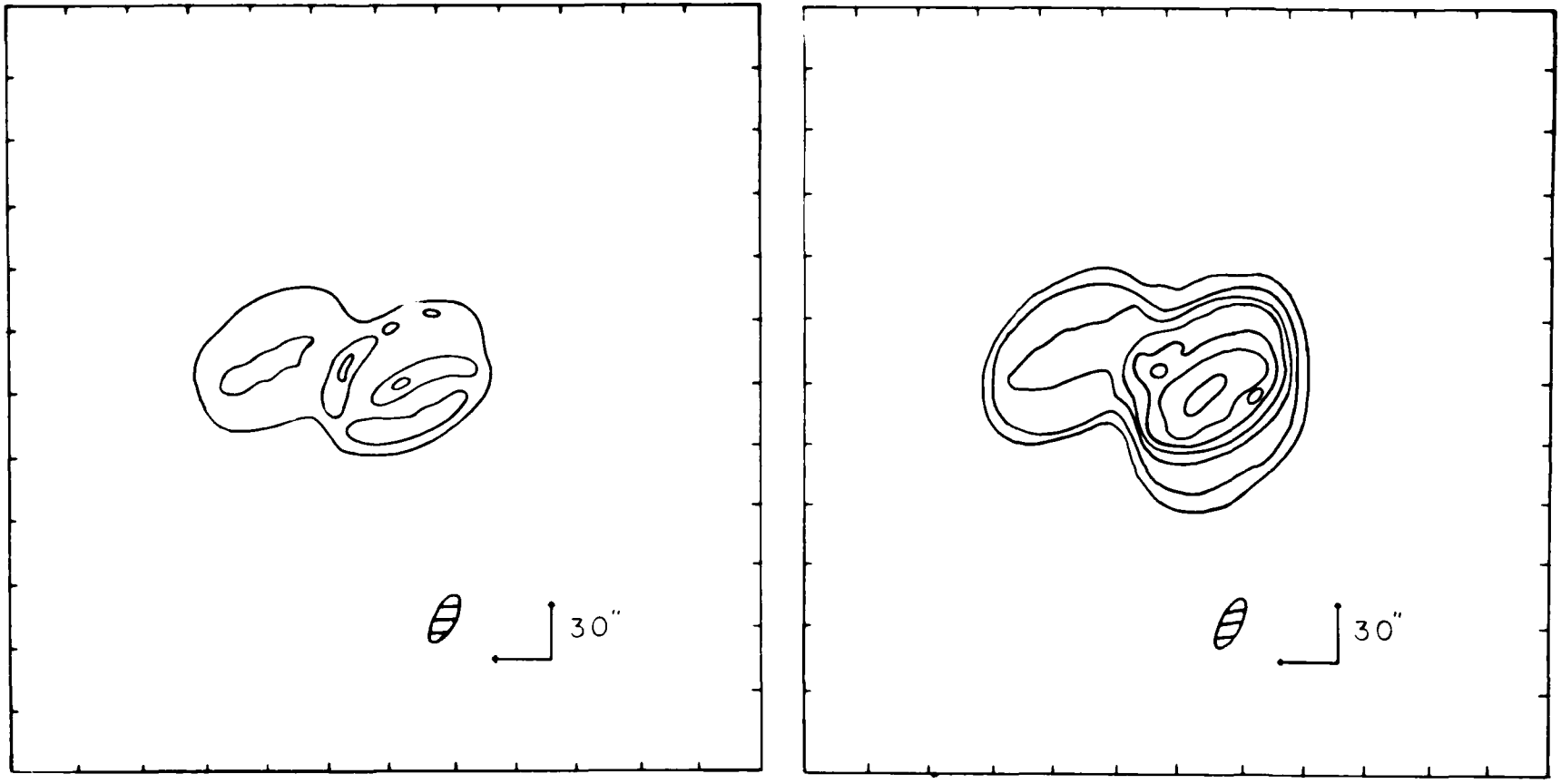

Figure 6. V.L.A. synthesis maps of the total intensity, I (right), and the circular polarization, V (left), at 6 cm wavelength of solar active region AR 2032 for one day's observation on October 5, 1979. North is up, East is to the left; dashed lines indicate negative values of V and correspond to right circularly polarized radiation, and solid lines denote positive V values and left circularly polarized radiation. The contours for the I map are at 35, 3σ, ...5Jy per square arc second. The maximum positive and negative values of the V contours are +15 and - 0 Jy per square arc second and the contour levels are also in steps of 5.

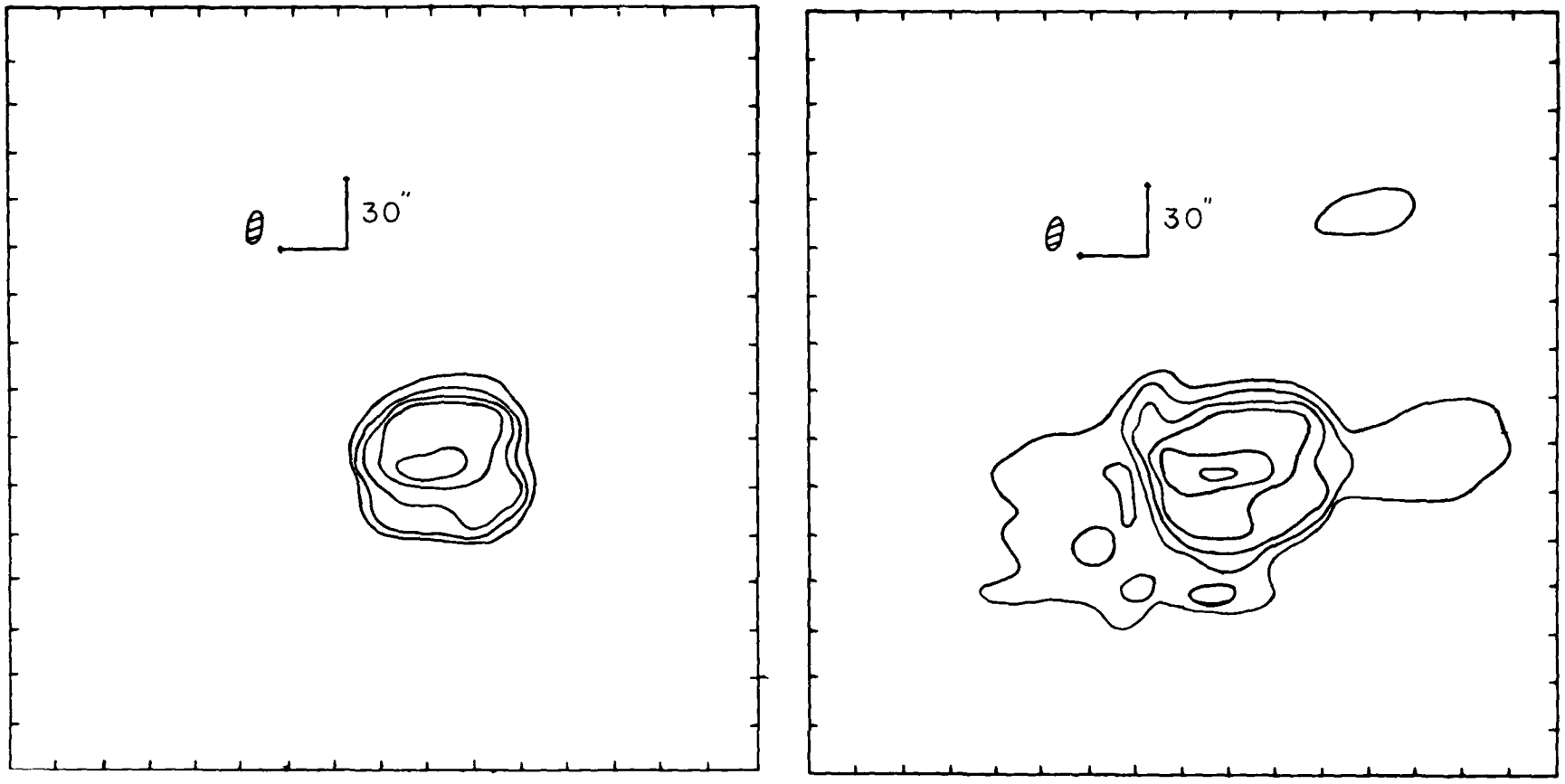

Figure 7. V.L.A. synthesis maps of the total intensity, I (right), and the circular polarization, V (left), at 6 cm wavelength of solar active region AR 2032 for one day's observation on October 6, 1979. North is up, East is to the left, dashed lines indicate negative values of V and correspond to right circularly polarized radiation, and solid lines denote positive V values and left circularly polarized radiation. The contours for the I maps are at 30, 25, ... 5 Jy per square arc second. The maximum positive and negative values of the V contours are +25 and - 0 Jy per square arc second and the contour levels are also in steps of 5 .

Section $_C$) which are also given in Table II. An optically thin condition is also suggested by the large degrees of circular polarization, p_c, for optically thick bremsstrahlung, for example, would exhibit no polarization. As indicated in Figures 1 through 7 and Table II, each of the bright regions of enhanced 6 cm emission also has one dominant magnetic polarity, and high circular polarizations which can vary from 30% to 100% within each source. Generally the brighter, optically thick regions tend to have lower polarizations, but the angular resolution was not adequate to map out this trend in detail. Future V.L.A. observations with the full array should result in the resolution of detailed features within each dominant source, and if our assumptions are correct the regions of highest brightness should exhibit this trend toward lower degrees of circular polarization. Although each active region also has one dominant magnetic polarity, many regions contain bright sources with opposite senses of circular polarization, suggesting the feet of magnetic dipoles. This suggests that the 6 cm maps of circular polarization act as coronal magnetograms which delineate the longitudinal magnetic fields of the solar corona.

When high resolution Hα photographs were available from the Air Force SOON network and N.O.A.A., we have used them for comparisons with the I synthesis maps on the same angular scale. As illustrated in Figures 8 to 13, there is an excellent correlation between enhanced emission of 6 cm wavelength and the chromospheric plage seen as bright regions on the Hα photographs. The maps of total intensity coincide in shape and orientation with the bright Hα emission, and the regions of enhanced 6 cm emission are confined within the boundaries of the bright Hα emission. Of special interest is Figure 8 which shows enhanced 6 cm emission without a depression in a region which contains bright Hα emission and a dark filament and Figures 11

Table II: Physical parameters for the circularly polarized cores given in order of decreasing intensity for each active region. Here we provide the peak value of the Stokes parameter, I, the corresponding brightness temperature, T_B, the peak value of the Stokes parameter, V, the degree of circular polarization p_c = peak I/(peak V), the estimated angular size, θ, and the emission measure $\int N_e^2 dl$ calculated under the assumption that the radiation is thermal bremsstrahlung at an electron temperature of $T_e = 2.5 \times 10^6$ K.* Note that the maps of I and V are given in units of Jy per synthesized beam area, that the peak I and peak V do not always coincide, and that p_c varies throughout each source.

Date	Active Region	Source	Peak I (Jy/"^{2})	T_B (10^6 K)	Peak V (Jy/"^{2})	p_c (%)	θ (")	$\int N_e^2 dl$ (10^{29} cm^{-5})
3/30/78	1046	1	35	1.8	+26	+74	20	4.3
	1046	2	35	1.8	+26	+74	20	4.3
	1046	3	15	0.8	-10	-67	10	1.9
4/1/78	1056	1	55	2.8	-40	-73	15	6.7
	1056	2	25	1.3	-13	-54	15	3.1
	1056	3	20	1.0	+13	+66	15	2.4
11/4/78	1374	1	80	4.1	+20	+25	30	9.8
	1374	2	30	1.6	-20	-67	$\lesssim$10	3.8
11/29/78	1407	1	52	2.7	+16	+30	20	6.4
	1407	2	41	2.2	+37	+88	20	5.2
	1407	3	31	1.6	-26	-84	$\lesssim$15	3.8
12/1/78	1429	1	215	11.2	+80	+37	30	26.6
10/5/79	2032	1	30	1.6	+ 8	+27	30	3.8
10/6/79	2032	1	38	2.0	+18	+47	45	4.8

*The calculated emission measures are uncertain by at least a factor of two because the electron temerature, T_e, is known to vary between 2 and 4 x 10^6 K, and the estimated brightness temperatures, T_B, in 1978 were also uncertain by at least a factor oftwo because of the weak calibration noise source of $\sim$ 4 K and the need to assume that the background temperature of the Sun is 2 x 10^4 K at 6 cm. In 1979 these uncertainties in T_B were removed by using stronger calibration noise sources.

and 12 where there is no detectable emission from sunspots and the enhanced 6 cm emission seems to outline loop-like structures whose features are outlined by bright chromospheric plage. All six figures indicate that when bright chromospheric plage is present, intense radio emission is also present; but there is no similar correlation with the presence or absence of sunspots. Our morphological comparisons indicate that active regions often contain several highly polarized sources which are associated with chromospheric plage, and that the brightest radio emission at 6 cm wavelength is not usually associated with sunspots at all. This opens up the possibility that the previously unresolved cores in the old (Kundu, 1959 a,b) core-halo model may be predominantly due to the bremsstrahlung of bright dense coronal condensations which lie in the regions between sunspots, and that gyroresonance absorption processes near sunspots may not play the dominant role at 6 cm wavelength.

When magnetograms of the solar photosphere were available from the Kitt Peak National Observatory (K.P.N.O.), we have compared them with the synthesis maps of circular polarization, V, on the same angular scale (Figures 14 to 18). Here, dark magnetogram areas refer to regions of negative magnetic polarity, and correspond to positive left hand circular polarization (solid lines) with the extraordinary mode of wave propagation. Similarly, light magnetogram areas refer to regions of positive magnetic polarity, and correspond to negative, right hand circular polarization (dashed lines) with the extraordinary mode of wave propagation. The comparisons given in Figures 14 to 18 indicate that the polarity, dipolar shapes, orientations and extents exhibited on the V maps are correlated with similar features seen in the magnetograms. The 6 cm maps of circular polarization and the Zeeman effect magnetograms respectively refer to the

Figure 9. A comparison of a V.L.A. synthesis map of total intensity, I, at 6 cm wavelength (see Fig. 3) with a U.S. Air Force SOON Hα picture on November 4, 1978 for solar active region AR 1374 (McMath 15635).

Figure 10. A comparison of a V.L.A. synthesis map of total intensity I, at 6 cm wavelength (see Fig. 4) with a U.S. Air Force SOON Hα picture on November 29, 1978 for solar active region AR 1407 (McMath 15073).

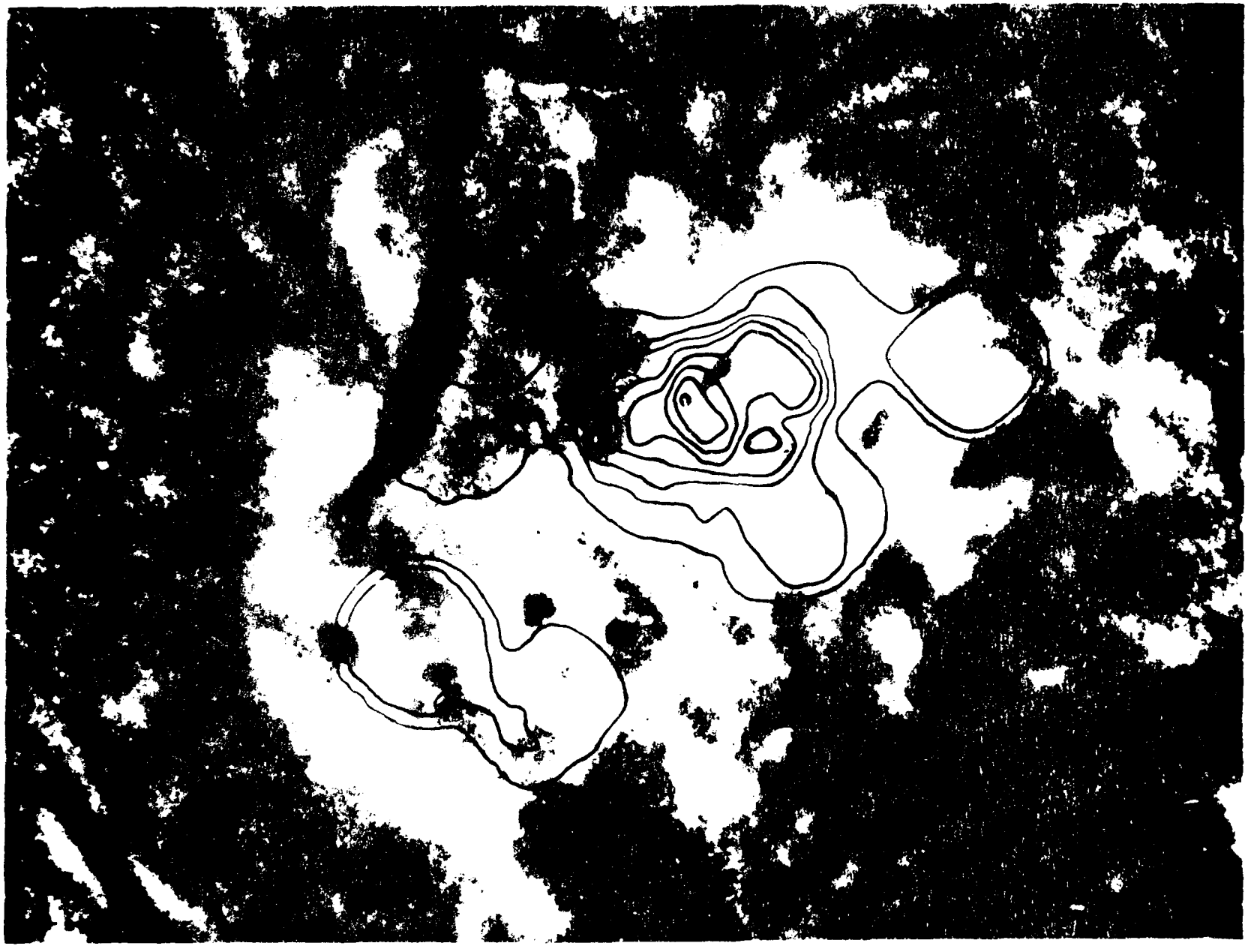

Figure 11. A comparison of a V.L.A. synthesis map of total intensity I, at 6 cm wavelength (see Fig. 5) with a U.S. Air Force 5000 Å picture on December 1, 1978, for the active region AR 1434.

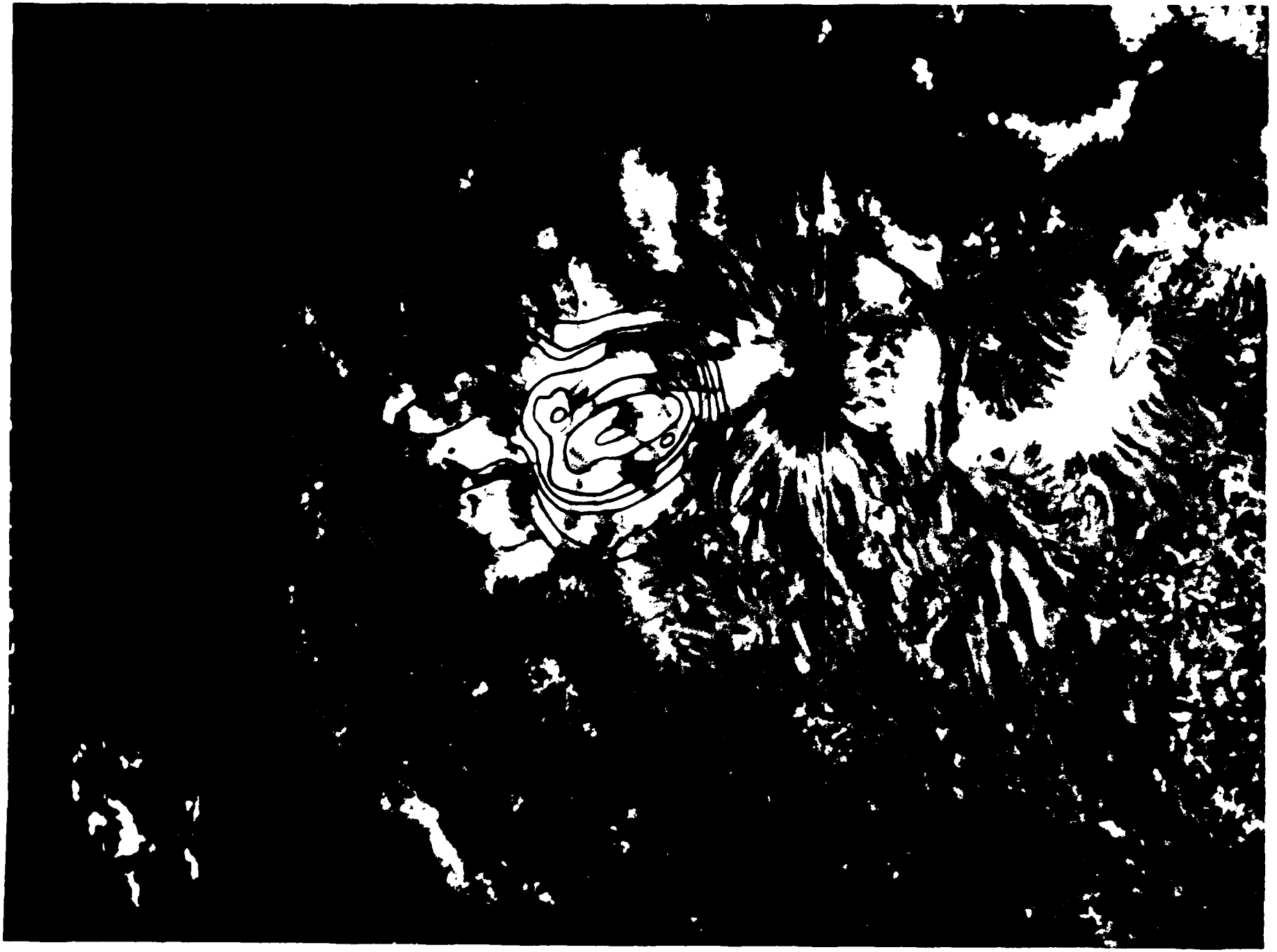

Figure 12. A comparison of a V.L.A. synthesis map of total intensity, I, at 6 cm wavelength (see Fig. 6) with a U.S. Air Force Sac B picture on October 3, 1979, for active region AR 2032.

Figure 13. A comparison of a V.L.A. synthesis map of total intensity, I, at 6 cm wavelength (see Fig. 7) with a U.S. Air Force S00N H_α picture on October 6, 1979 for active region AR 2032. In this case, a detailed morphological comparison with greater angular resolution has been given by Felli, Lang and Willson (1980).

longitudinal component of the magnetic field in the low solar corona and the underlying solar photosphere. The correlation between the V maps and the magnetograms suggests that the former delineate regions in which the photospheric field is projected vertically upwards into the low solar corona, as first suggested by Lang and Willson (1979, 1980). The correlation indicates an intimate connection between enhanced radio emission and intense magnetic fields which are not necessarily directly associated with sunspots. When loop-like structures are apparent, however, the hot plasma seen at Hα, radio and X-ray wavelengths may well be trapped in the arches of magnetic loops which are sometimes connected to sunspots.

Figure 14. A comparison of a V.L.A. synthesis map of circular polarization, V, at 6 cm wavelength (see Fig. 1) with a K.P.N.O. magnetogram taken on March 30, 1978 for active region AR 1046 (McMath 15205). The dark regions of the magnetograms refer to regions of negative magnetic polarity and correspond to positive V values (solid contours) and left circularly polarized radiation at 6 cm. The light regions of the magnetograms refer to regions of positive magnetic polarity and correspond to negative V values (dashed contours) and right hand circularly polarized radiation at 6 cm. The magnetograms are enlargements of the appropriate sections of the K.P.N.O. full disk magnetograms.

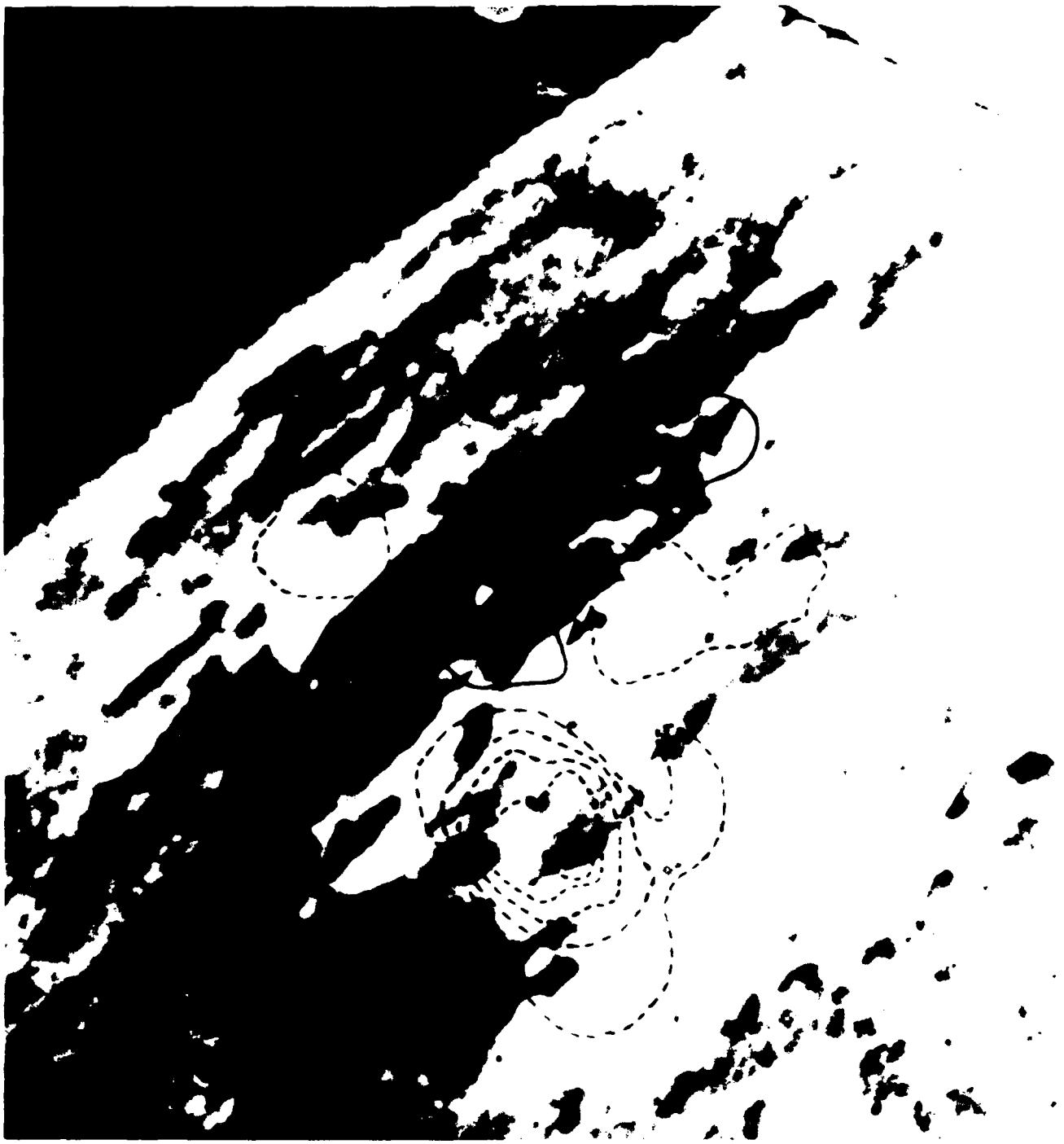

Figure 15. A comparison of a V.L.A. synthesis map of circular polarization, V, at 6 cm wavelength (see Fig. 2) with a K.P.N.O. magnetogram taken on April 1, 1978, for active region AR 1056 (McMath 15220). The dark regions of the magnetograms refer to regions of negative magnetic polarity and correspond to positive V values (solid contours) and left circularly polarized radiation at 6 cm. The light regions of the magnetograms refer to regions of positive magnetic polarity and correspond to negative V values (dashed contours) and right hand circularly polarized radiation at 6 cm. The magnetograms are enlargements of the appropriate sections of the K.P.N.O. full disk magnetograms.

Figure 16 mparison of a V.L.A. synthesis map of circular polarization, V, at 6 cm wavelength (see Fig. 3) with a K.P.N.O. magnetogram taken on November 4, 1978 for active region AR 1374 (McMath 15634). The dark regions of the magnetograms refer to regions of negative magnetic polarity and correspond to positive V values (solid contours) and left circularly polarized radiation at 6 cm. The light regions of the magnetograms refer to regions of positive magnetic polarity and correspond to negative V values (dashed contours) and right hand circularly polarized radiation at 6 cm. The magnetograms are enlargement of the appropriate regions of the K.P.N.O. full disk magnetograms.

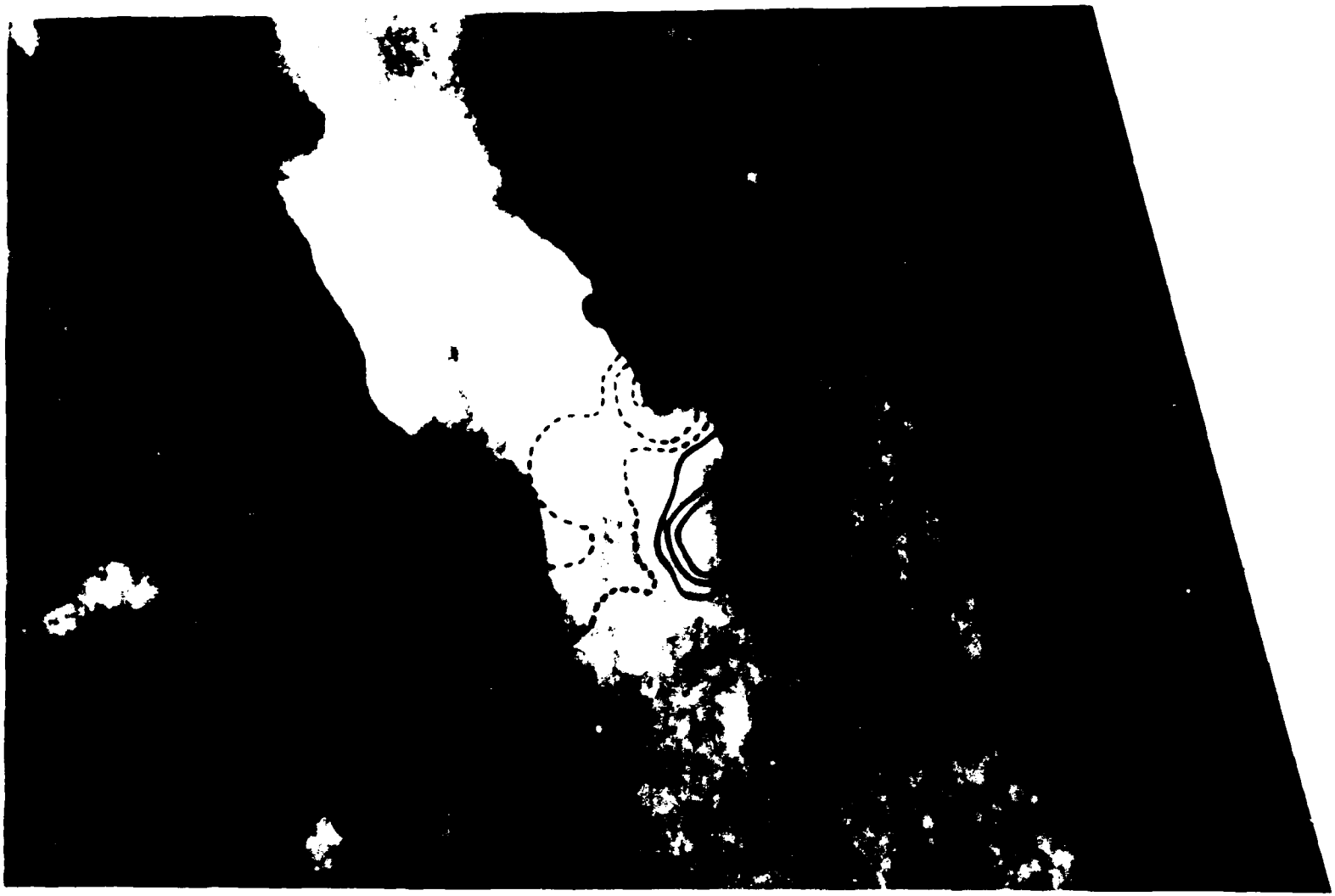

Figure 17. A comparison of a V.L.A. synthesis map of circular polarization, V, at 6 cm wavelength (see Fig. 4) with a K.P.N.O. magnetogram taken on November 29, 1978 for active region AR 1407 (McMath 15673). The dark regions of the magnetograms refer to regions of negative magnetic polarity and correspond to positive V values (full contours) and left circularly polarized radiation at 6 cm. The light regions of the magnetograms refer to regions of positive magnetic polarity and correspond to negative V values (dashed contours) and right hand circularly polarized radiation at 6 cm. The magnetograms are enlargements of the appropriate sections of the K.P.N.O. full disk magnetograms.

[illegible] comparison of a [illegible] synthesis map of circular polarization, V, at 6 cm wavelength (see Fig. 7) with [illegible] magnetograms taken on October 6, 1979 for active region AR 2032. The dark regions of the magnetograms refer to regions of negative magnetic polarity and correspond to positive V values [illegible] left circularly polarized radiation at 6 cm. The light regions of the magnetograms [illegible] positive magnetic polarity and correspond to negative V values (dashed contours) and [illegible] polarized radiation at 6 cm. The magnetograms are enlargements of the appropriate [illegible] magnetograms.

C. OWENS VALLEY OBSERVATIONAL RESULTS

Another phase of our work, more directly related to the prediction of solar flares, was the monitoring of active regions for changes in the microwave circular polarization which reflect the emerging magnetic fields which can trigger subsequent flare emission. It is generally believed that magnetic fields in the low solar corona are disrupted prior to the emission of solar flares and there is already some evidence that these flare precursors can be detected in the centimeter wavelength emission from the relevant active region, and that the emission of flares may be correlated with a particular spatial distribution of this radio radiation. Lang (1977) has shown that the emission of solar flares is preceded by an increase in the polarization, as well as the intensity, of the centimeter wavelength radiation of active regions. He showed that the normal day long stability of the radio sources is disrupted by changes in polarization of up to one hundred percent at time intervals between a few minutes and many tens of minutes before the eruption of solar flares. Alissandrakis (1977) has also observed that the circular polarizaton of centimeter wavelength radiation reaches a maximum several minutes before the emission of flares seen at optical wavelengths. All of these radio wavelength observations suggest that stronger or more ordered coronal magnetic fields may act as a flare trigger mechanism. By monitoring active regions over several weeks, our hope was to extend these pioneering observations and to gather a large enough data base in order to be able to detect patterns in the circular polarization changes which might serve as signatures for the commencement of flare activity. Because of the unpredictable occurrence of microwave bursts and because only a limited amount of observing time is available on the Very Large Array instrument

we decided to carry out these observations using the Caltech two-element interferometer at Owens Valley where long periods of time are available. This instrument also has the capability of sampling the signals at a very rapid rate (once every 50 milliseconds) thereby making it possible to study the polarization properties of a burst with high time resolution.

The observations described in this section were made during a two week period between December 4 and December 16, 1979. The interferometer consisted of two 85 foot parabaloids separated by 200 meters along an east-west direction. At our operating wavelength of 2.8 cm, the individual antenna beamwidths are $\sim$6 minutes of arc and the interferometer fringe spacing is $\sim$30 seconds of arc. In order to study the suspected rapid polarization changes with maximum time resolution, the left and right circularly polarized signals were sampled at the fastest possible rate of once every 50 milliseconds. The instrumental gain and polarization were calibrated by observing the extragalactic sources 3C273 and 3C345 about once per hour.

Our general observing plan was to track a particular active region for as long as it was suspected to have a good chance of flaring. This strategy allowed us to study the development of the region's polarization characteristics over several days. The results of our observations are summarized in Tables III and IV where in Table III we list the regions and times that they were observed and in Table IV we list the flares that were detected, their intensities, and the circular polarizations both before and during the flares. The left and right circularly polarized amplitudes were first examined by plotting every 50 millisecond data point and were later averaged over a 5 second interval when it was found

that, to within the noise, no structure could be detected on a timescale shorter than this value. In all, 14 events were detected. In Figures 19-24 we have plotted as a function of universal time the Stokes parameters I = (LCP + RCP)/2 , V = (LCP-RCP)/2 , and the circular polarization p = V/I , for six of the flares, where LCP and RCP refer to the left and right circularly polarized signals.

As Table IV and Figures 19-24 show, all of the events were of weak to moderate intensity (1 to 10 solar flare units) and each lasted between 1 to 10 minutes. Most of the flares also exhibit the "classical" emission profile, characterized by a rapid rise in intensity to a maximum followed by a slower decline. In almost every case the preflare circular polarization was about 50 percent whereas the change in polarization during the burst was typically less than 20 percent.

Of particular interest is the strongest flare which occurred at 1923 UT on December 8 and which we illustrate in Figure 19. The radio burst was associated with an Hα event originating in active region AR2159, located approximately 5 minutes of arc from the region being tracked on that day, AR2156. The circular polarization begins to change about three minutes before the total intensity reaches a maximum, changes sign and peaks at the same time as the total intensity, then declines to its preflare value during the post-impulsive phase. This type of polarization variation is different from that found by Kundu and Vlahos (1979) who observed that, at 6 cm wavelength, bursts of moderate to weak intensity were polarized only in the impulsive phase and only in one sense of polarization. For those flares, they claimed that if the emission arose from a bipolar loop structure, then the emission must be associated with only one leg of the loop. That the flare on December 8 (and most of the

others observed by us) is seen at both right and left circular polarizations seems to indicate that the burst originates from opposite magnetic polarities of the loop. It is also possible to infer that the optical thickness, τ, of the bursting source, is less than or equal to unity throughout the flare since as equation 4 of the next section shows, optically thick radiation $\tau >> 1$, is unpolarized even in the presence of a magnetic field.

As Figures 19-24 illustrate, there were no dramatic changes occurring several minutes before the flares. In order to see if such changes might have occurred on larger time scales, i.e., of several tens of minutes to an hour before the flares, we show in Figures 25-29 plots of the V stokes parameter and of the circular polarization, p, for times of up to two hours before and after the events. Again, these figures show that there are no obvious impulsive (i.e., timescales of a few minutes) polarization changes on hourly timescales which one would immediately identify as a "precursor". There are, however, indications of more gradual variations such as those which occur before, during and after the flares on December 14 (Figure 27) and 16 (Figure 29). On December 14, for example, the pre-flare emission was about 70 percent left circularly polarized, decreased to $\sim$20 percent after the flare at 1842 UT, then increased to about 40 percent about 3.5 hours later and before the last three events seen on that day. A similar and somewhat more abrupt ($\sim$1 hour) change was detected before, during and after the bursts at 1644 and 1706 UT on December 16.

These results suggest that rapid pre-flare polarization changes of the type previously reported, do not always precede flare activity. More moderate variations with amplitudes on the order of 30-40 percent on timescales of about an hour are sometimes seen around the times of flares.

TABLE III

SUMMARY OF OWENS VALLEY OBSERVATIONS

Date	Active Region	Time Observed (UT)
12-4-79	2164	1800-2327
12-5-79	2164	1630-2334
12-6-79	2164	1708-1745
	2156	2258-2334
12-7-79	2156	1620-2325
12-8-79	2156	1610-2327
12-9-79	2156	1616-2325
12-10-79	2156	1613-1820
	2176	1826-2324
12-11-79	2162	1626-1926
	2176	1957-2327
12-12-79	2176	1622-2325
12-13-79	2191	1657-2333
12-14-79	2186	1620-2327
12-15-79	2186	1616-2325
12-16-79	2186	1615-2142

TABLE IV

Summary of Flares Observed at OVRO 2.8 cm

Date	Region	Begin	End	Peak	Pre-Flare		Flare	
					Flux (SFU)	Pol	Flux (SFU)	Pol
12/8/79	AR2159	1922	1923	1925	0.97	-0.09	8.9	0.31
12/9/79	AR2156	1658	1659	1700	0.87	0.39	1.52	0.32
12/9/79	AR2156	1717	1718	1718	0.81	0.43	1.01	0.39
12/9/79	AR2156	1739	1740	1742	0.79	0.41	1.68	0.36
12/9/79	AR2156	1904	1904	1941	0.79	0.38	1.46	0.31
12/12/79	AR2176	1713	1714	1715	0.44	-0.56	0.89	-0.26
12/14/79	AR2186	1838	1842	1850	0.29	0.42	0.59	0.40
12/14/79	AR2186	2251	2252	2253	0.42	0.59	0.75	0.54
12/14/79	AR2186	2258	2259	2300	0.54	0.52	0.76	0.50
12/14/79	AR2186	2307	2307	2309	0.60	0.53	1.03	0.43
12/15/79	AR2186	1958	1959	2000	0.46	0.38	0.82	0.45
12/16/79	AR2186	1644	1644	1649	0.84	-0.54	1.86	-0.24
12/16/79	AR2186	1705	1706	1708	0.62	-0.27	1.49	-0.19
12/16/79	AR2186	2123	2127	2129	0.54	0.54	1.70	0.08

It should be kept in mind, however, that nearly all of the flares detected in this study were of weak ($\sim$1 SFU) intensity and there may be a threshold below which polarization changes caused by the emergence or reordering of coronal magnetic fields may be undetectable. Further studies during a time when the sun in more active would be useful to confirm this.

We caution, however, that it is often difficult, when using a single interferometer baseline, to distinguish between polarization variations that are caused by the reordering of coronal magnetic field structure from those changes that are caused by variations of the fringe amplitude of a highly polarized active region. Multiple wavelength observations of solar flares with the Very Large Array would of course be of great value since they would provide the positions, sizes, brightness and polarization structures of the bursts during both the impulsive and post-burst phases with second of arc resolution. This information could be used to test certain ambiguous interpretations of the bursts which already appear in the literature. Alissandrakis and Kundu (1978), for example, have used Westerbork observations to suggest that the 6 cm burst sources at first contract until the maximum burst intensity is reached and then expand during the post-burst phase. It is difficult to see how one can compress the magnetic field lines, however, and it may be that an apparent compression is produced by the faster rise of the smaller components. Multiple wavelength V.L.A. observations could simultaneously sample the bursts at a variety of heights and thereby help resolve this ambiguity of source expansion and contraction. It would also be possible to measure the polarization at

different heights and thereby test the prevalent view that the unpolarized or weakly polarized post-burst phase represents the thermalization of the non-thermal electrons of the impulsive phase by collision with particles in the ambient plasma.

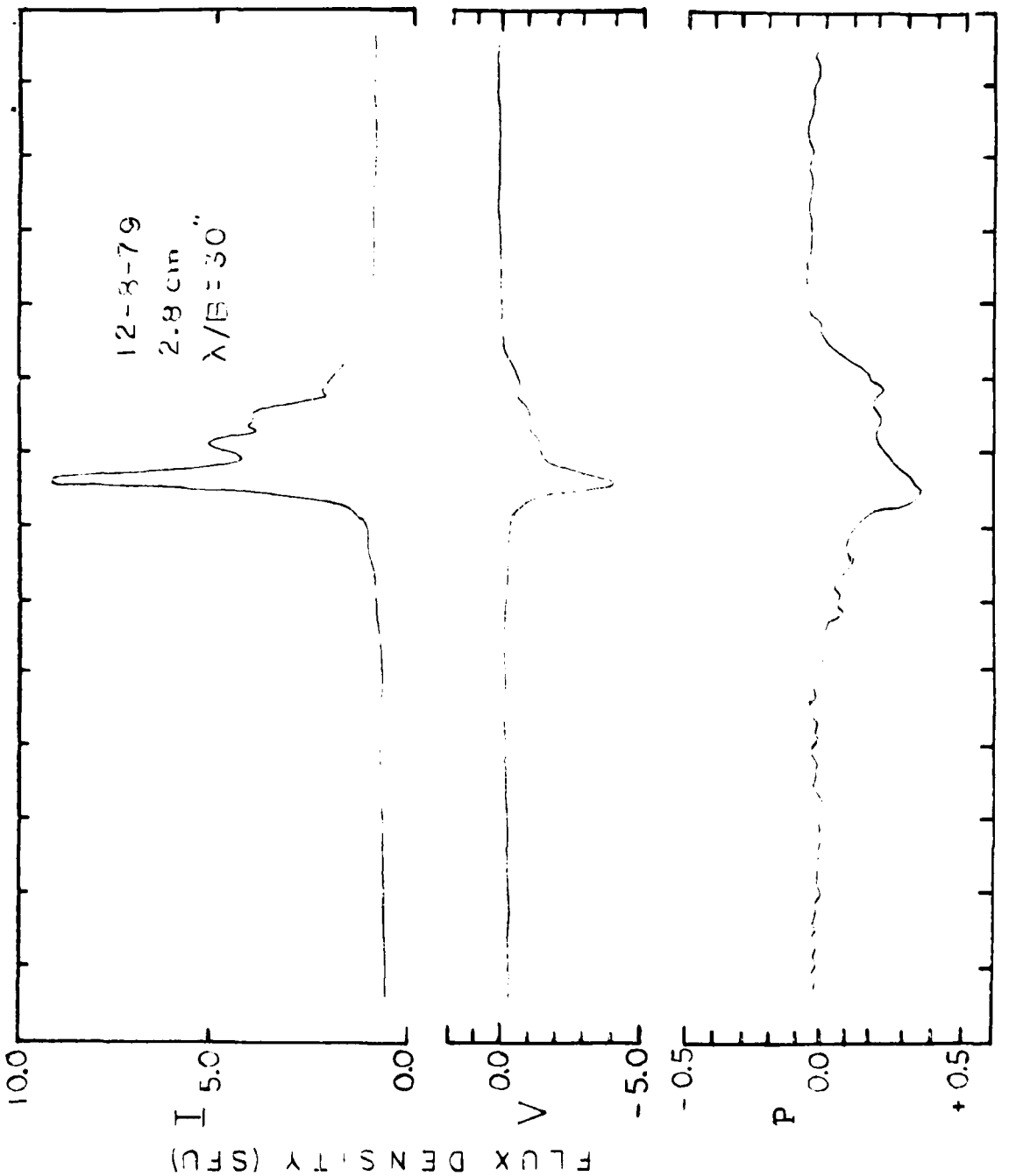

Figure 19. The total intensity, I (top), the circular polarization, V (middle), and the polarization percentage p, (bottom), plotted as a function of Universal Time for a burst on December 8, 1979.

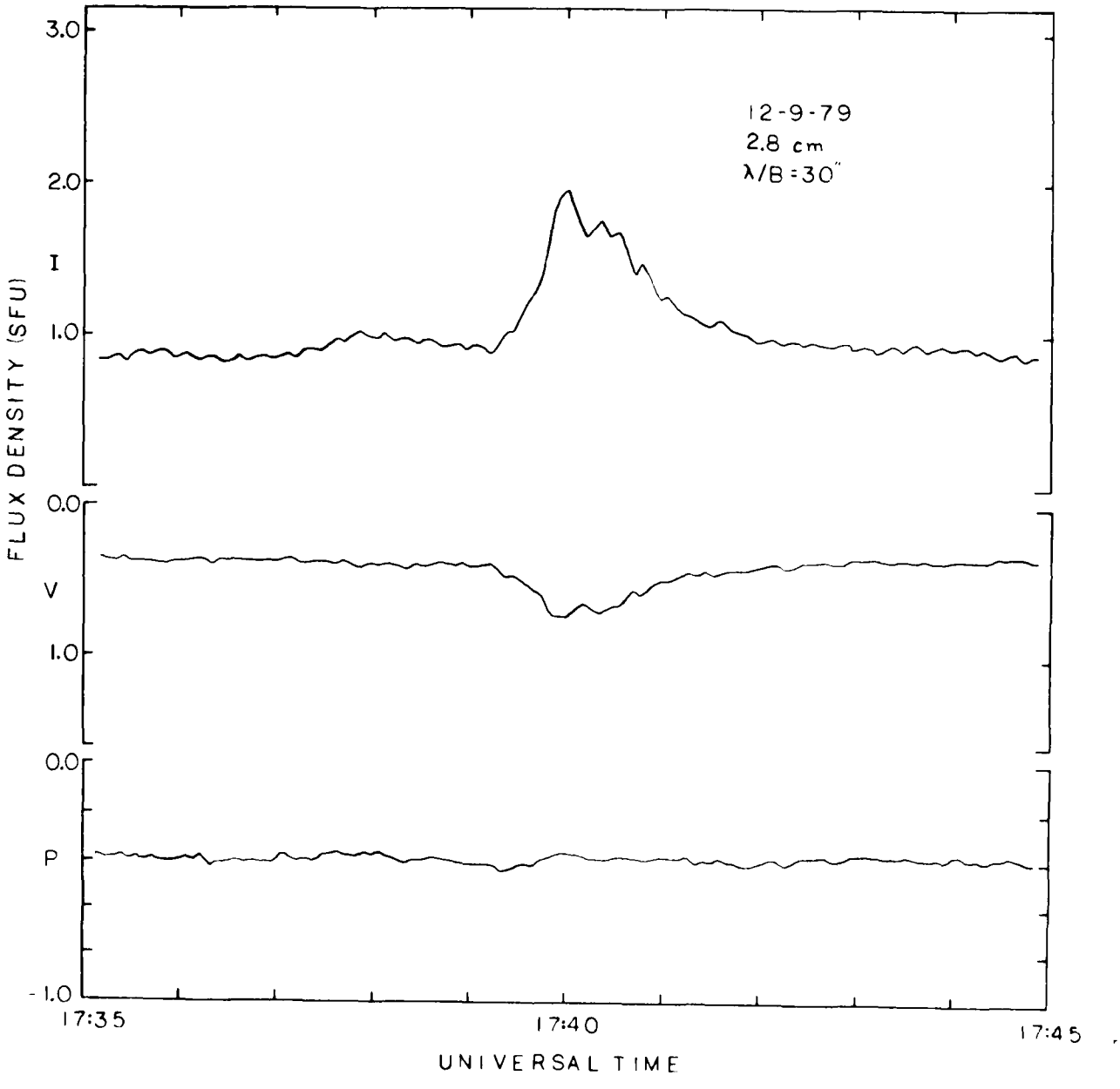

Figure 20. The total intensity, I (top), the circular polarization, V (middle), and the polarization percentage, p (bottom), plotted as a function of Universal Time for a burst on December 9, 1979.

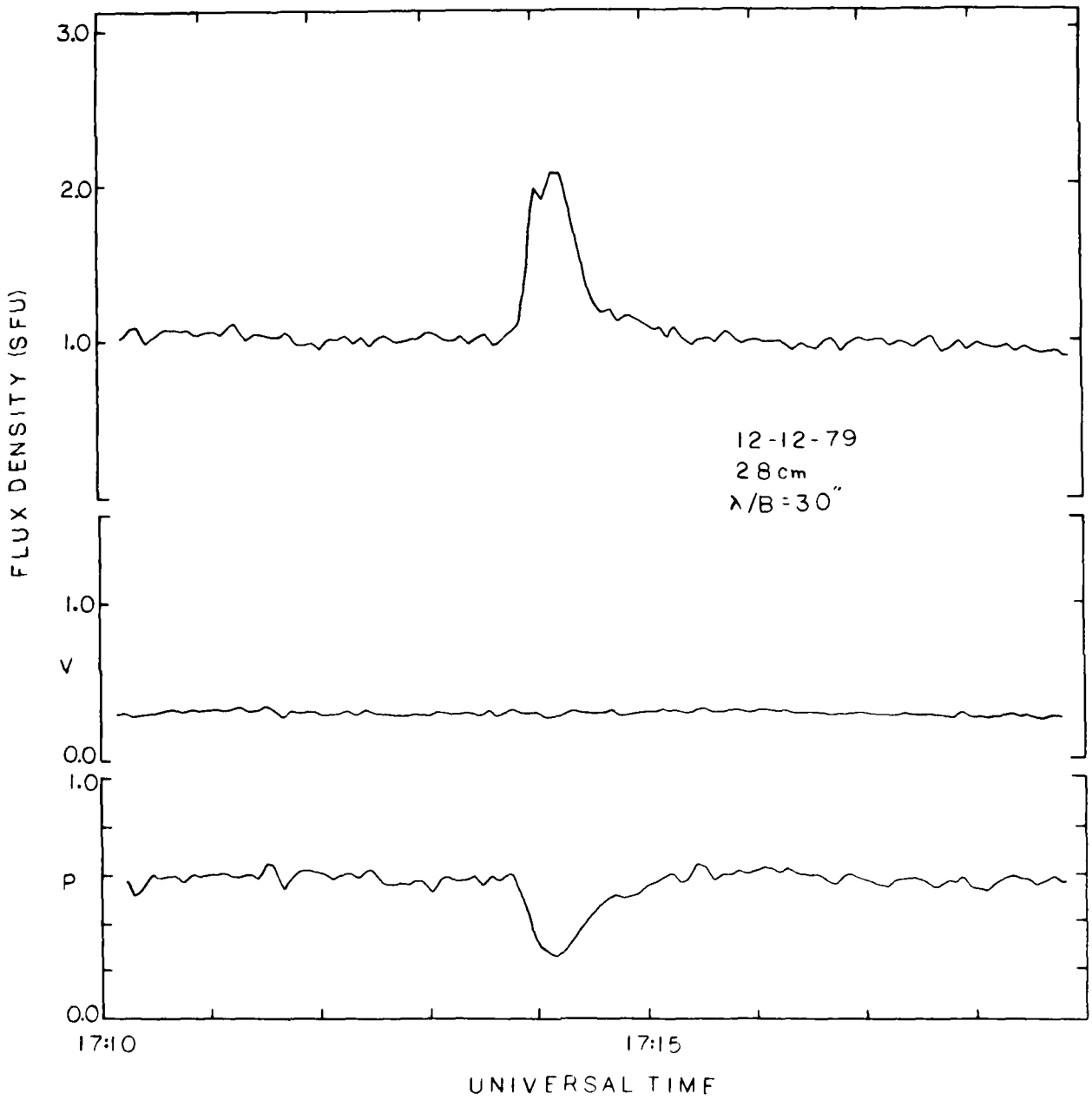

Figure 21. The total intensity,I (top), the circular polarization,V (middle), and the polarization percentage,p (bottom) plotted as a function of Universal Time for a burst on December 12, 1979.

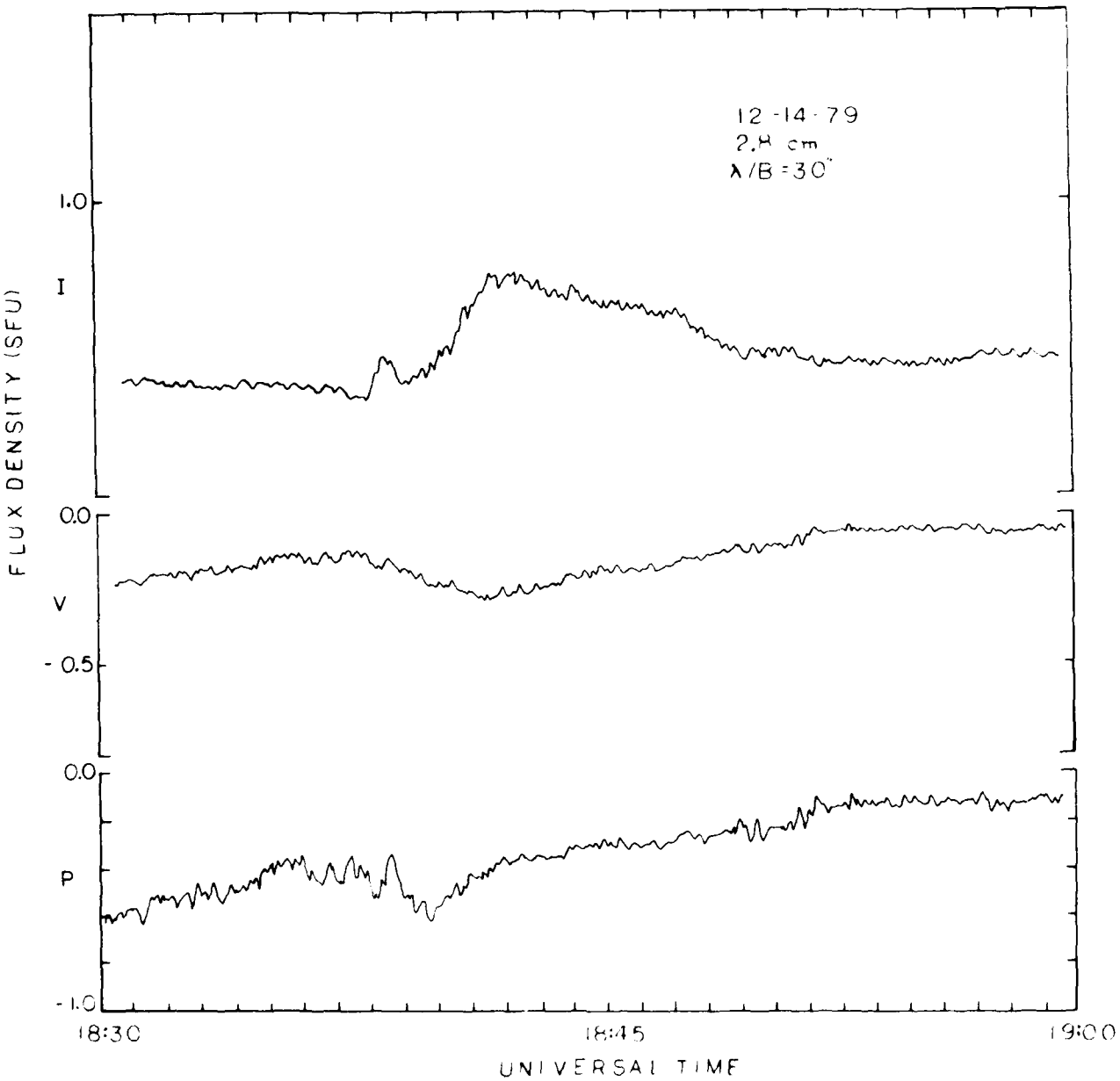

Figure 22. The total intensity, I (top), the circular polarization, V (middle), and the polarization percentage, p (bottom), plotted as a function of Universal Time for a burst on December 14, 1979.

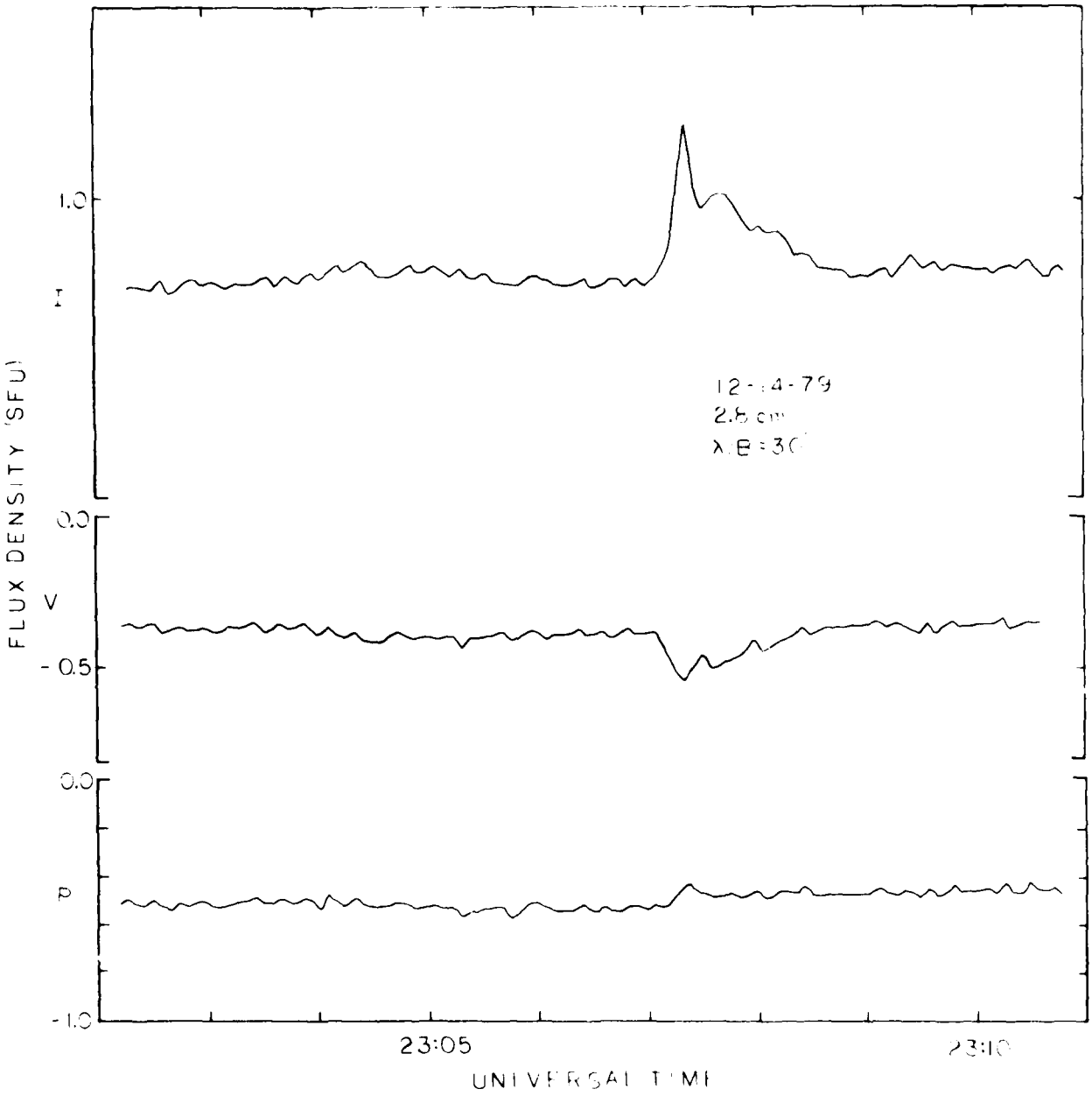

Figure 23. The total intensity, I (top), the circular polarization, V (middle), and the polarization percentage, p (bottom), plotted as a function of Universal Time for a burst on December 14, 1979.

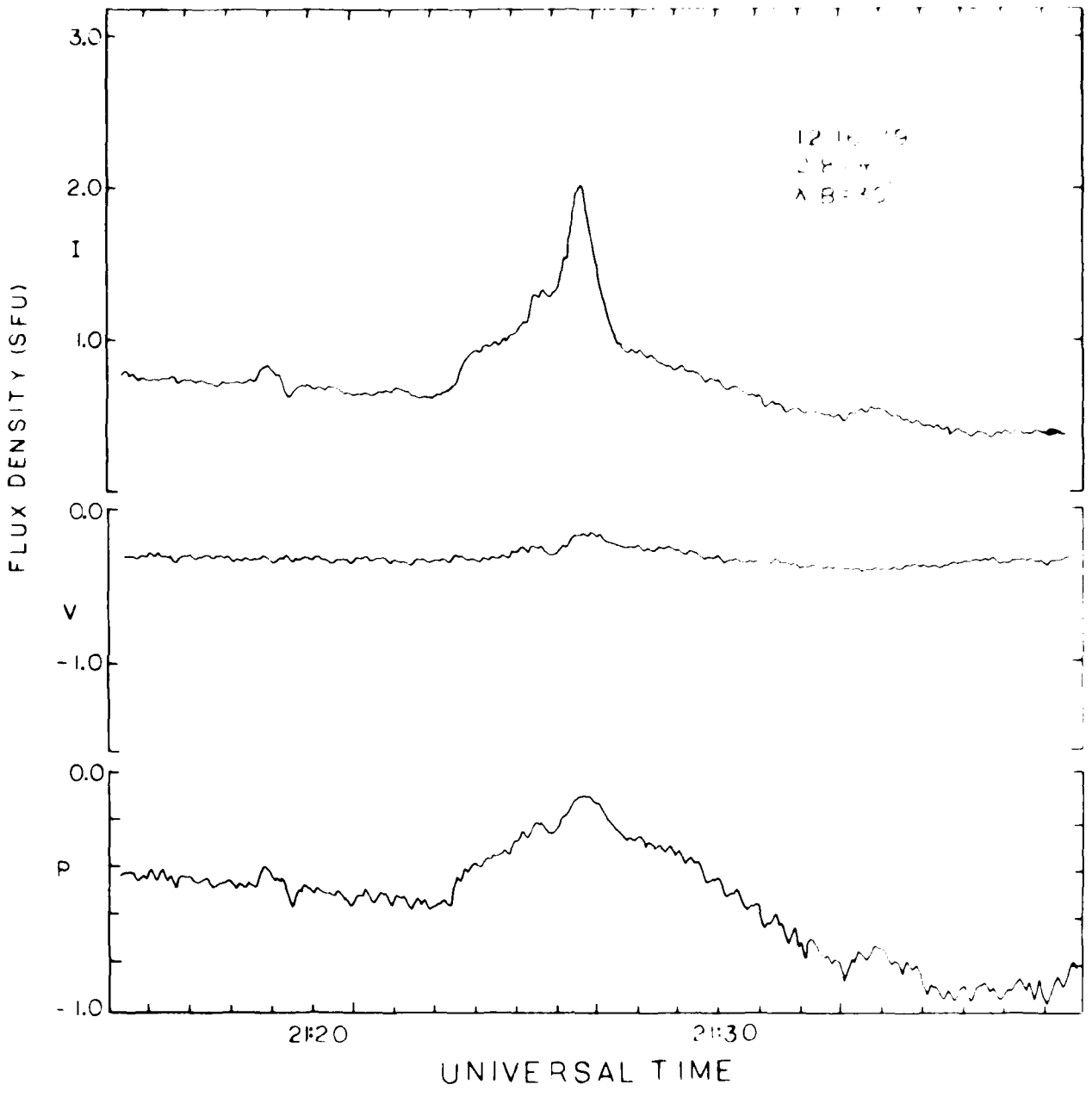

Figure 24. The total intensity, I (top), the circular polarization, V (middle), and the polarization percentage, p (bottom), plotted as a function of Universal Time for a burst on December 16, 1979.

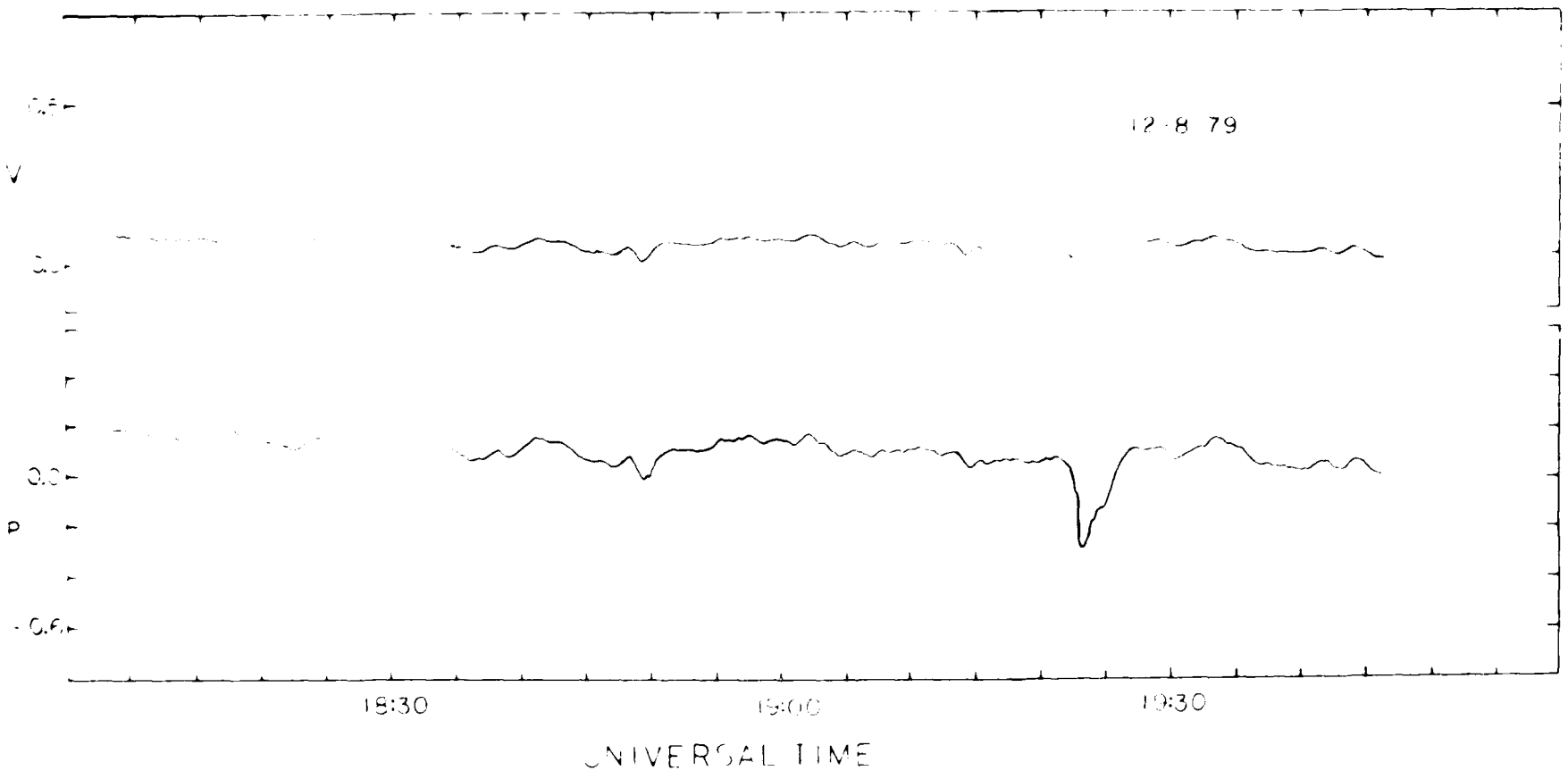

Figure 25. The circular polarization, V (top) , and the polarization percentage, p (bottom), plotted as a function of Universal Time on December 8,1979.

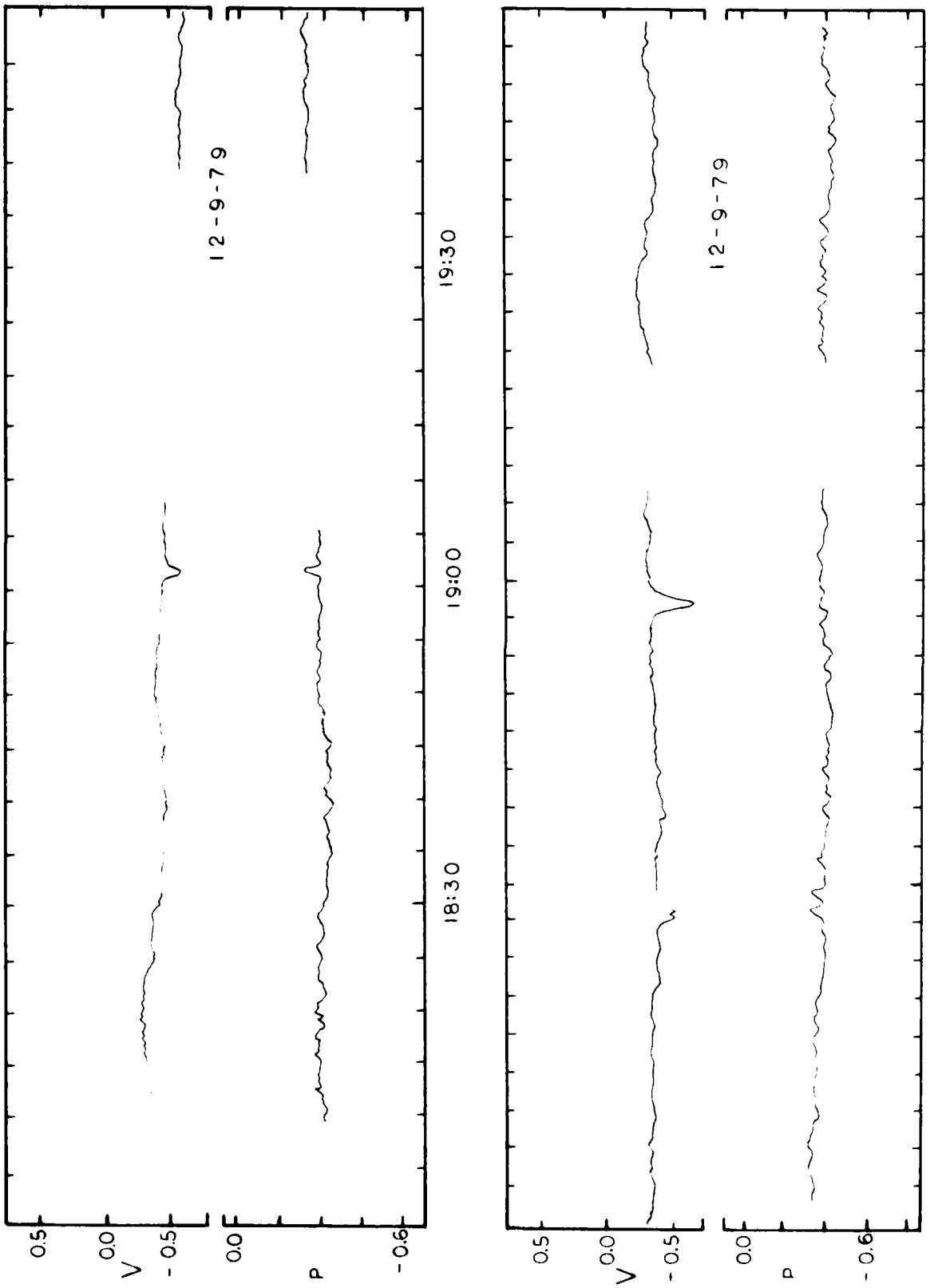

Figure 26. The circular polarization, V (top), and the polarization percentage, p (bottom), plotted as a function of Universal Time on December 9, 1979.

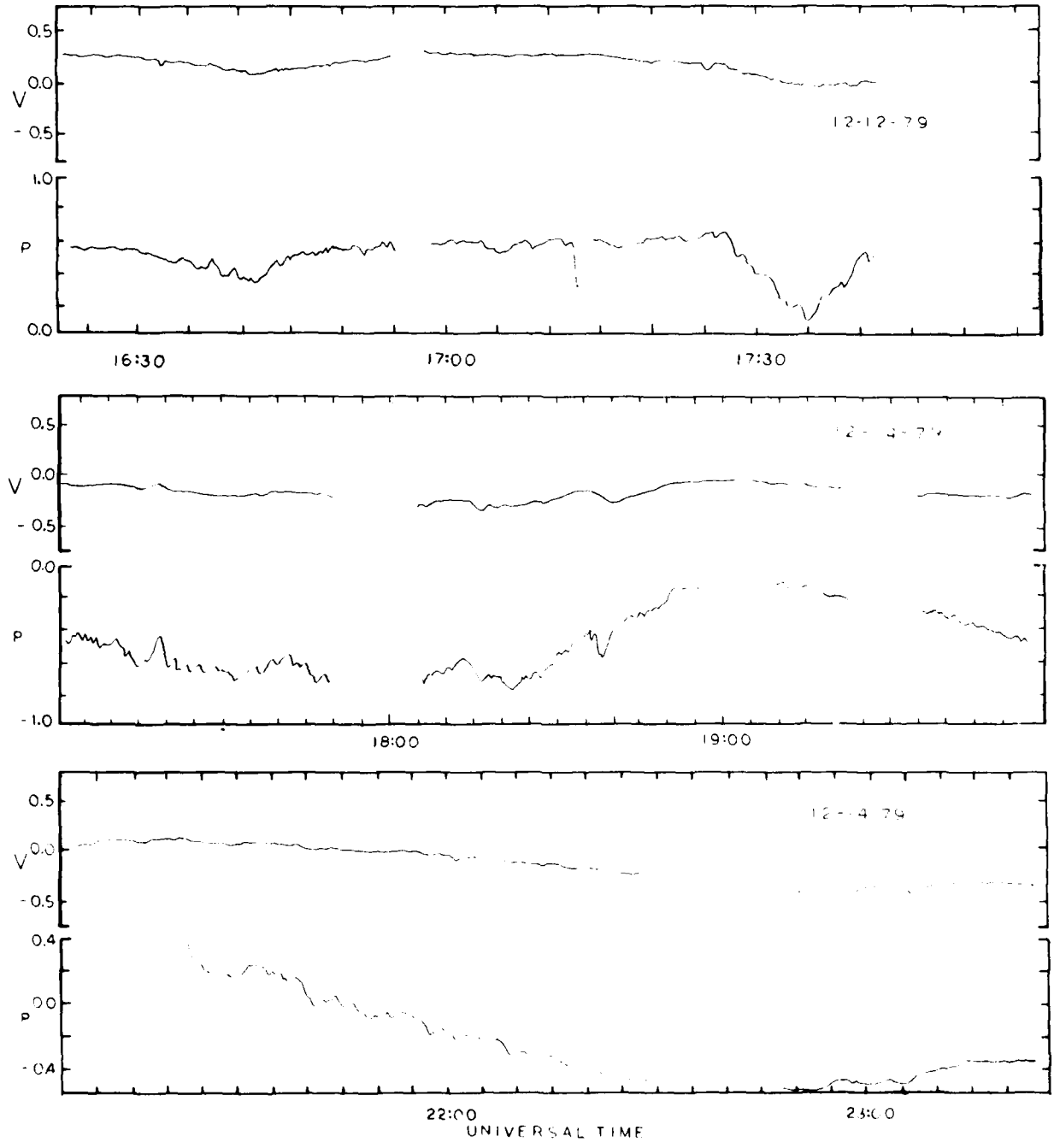

Figure 27. The circular polarization, V (top), and the polarization percentage, p (bottom), plotted as a function of Universal Time on December 12 and 14, 1979.

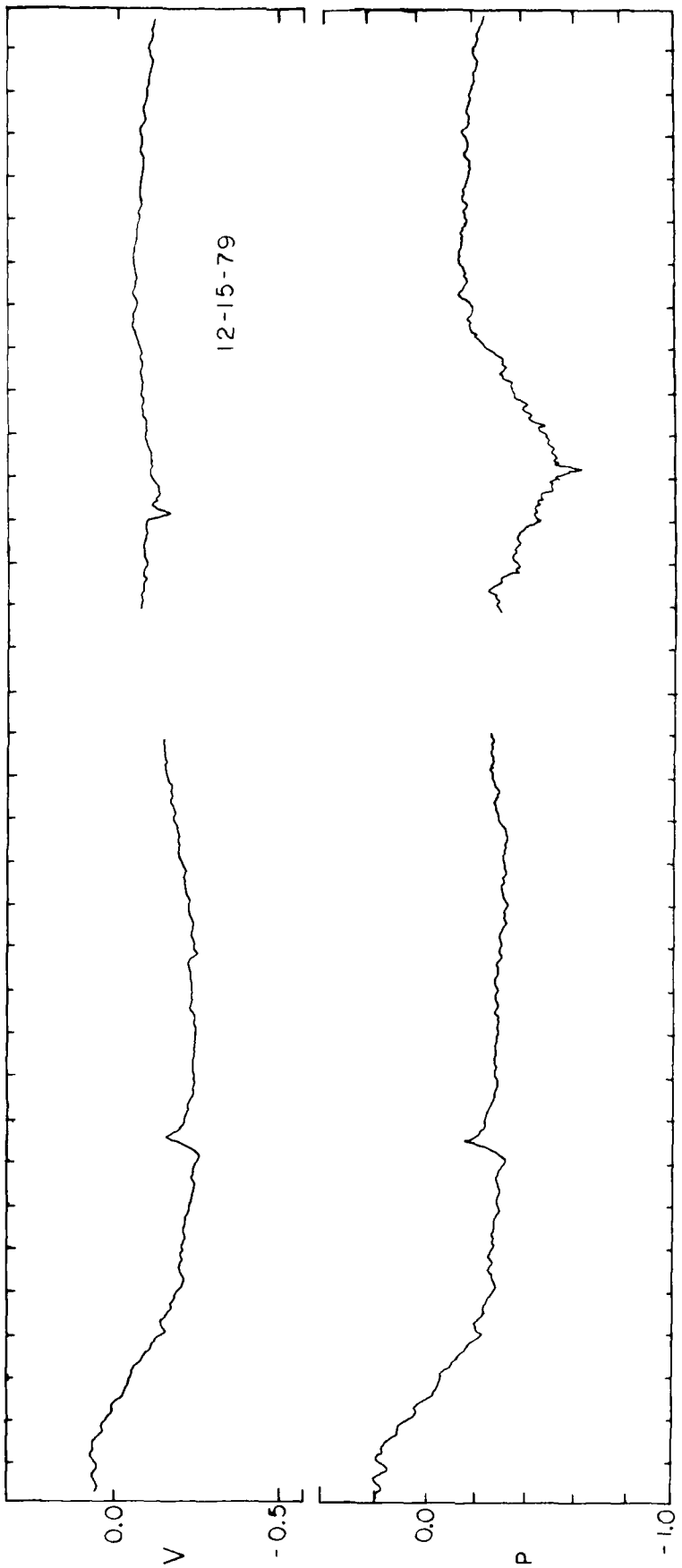

Figure 28. The circular polarization, V (top), and the polarization percentage, p (bottom), plotted as a function of Universal Time on December 15, 1979.

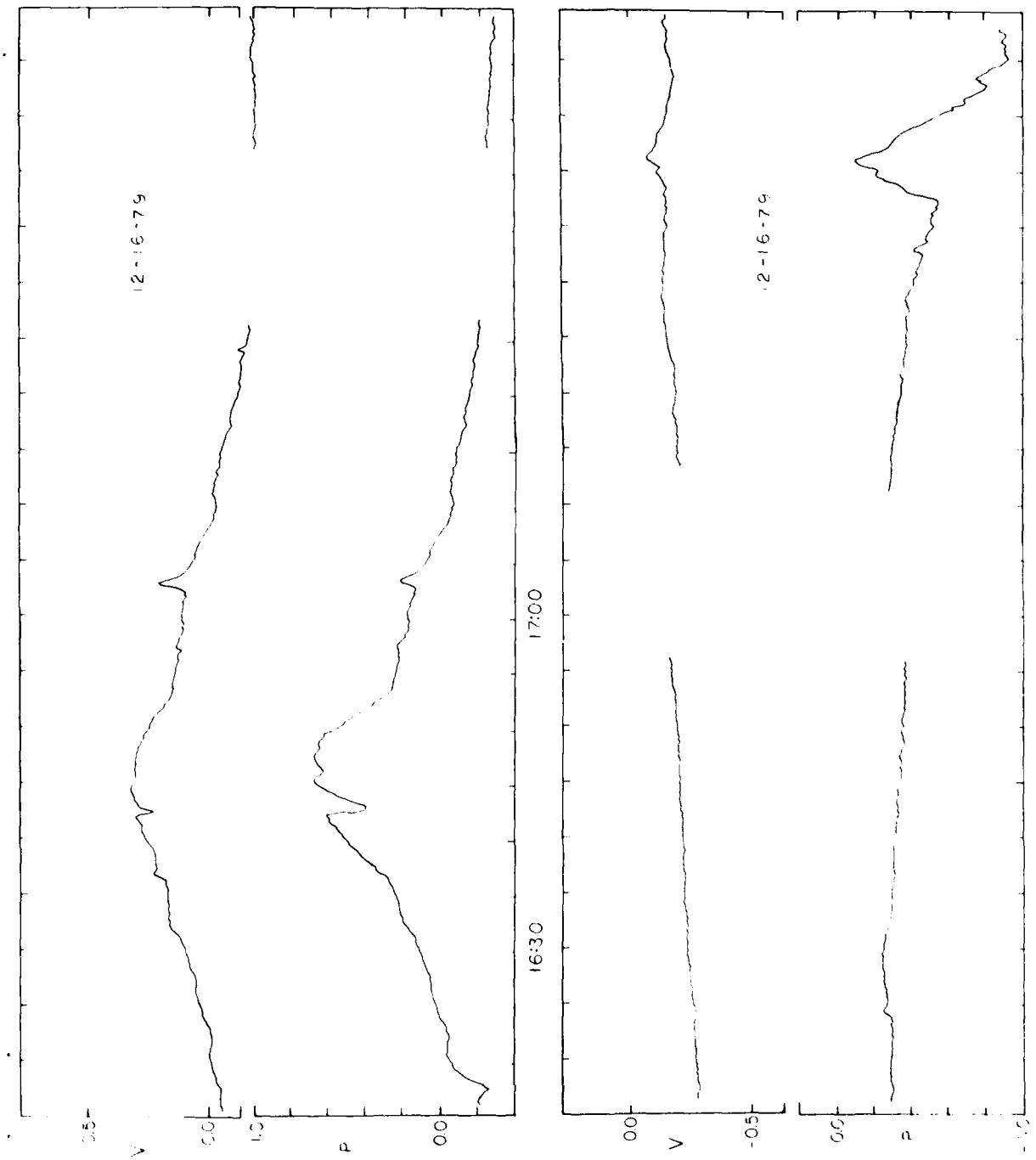

Figure 29. The circular polarization, V (top), and the polarization percentage, p (bottom), plotted as a function of Universal Time on December 16, 1979.

THEORETICAL DISCUSSION

In Section II we have presented observations of six different active regions at widely different times, and these data provide a reasonably large sample for testing the possible radiation mechanisms which may account for the enhanced radio emission detected at 6 cm wavelength. The observed emission has average brightness temperatures of $T_B \gtrsim 10^6$ K, for example, and these temperatures imply representative optical depths of $\tau \gtrsim 0.3$ for the electron temperatures of $T_e = 2$ to 4×10^6 K which are known to exist in the coronal atmosphere above active regions. Under the assumption that the observed radiation is due to thermal electrons of electron density, N_e, and electron temperature, T_e, there are two sources of opacity which are respectively due to the bremsstrahlung interactions of the electrons with ions and the gyromagnetic interaction of the electrons with magnetic fields. The optical depth, τ_B, for bremsstrahlung (braking or free-free radiation) which applies at radio wavelengths for temperatures exceeding 3×10^5 K is given by (Lang 1974b, 1980):

$$\tau_B = 9.786 \times 10^{-3} \frac{\int N_e^2 d\ell}{\nu^2 T_e^{3/2}} \ln \left[4.7 \times 10^{10} \frac{T_e}{\nu}\right]$$

$$\approx 1.68 \times 10^{-30} \int N_e^2 \, d\ell \; ; \qquad (1)$$

whereas the optical depth, τ_G, for gyroresonance absorption is (Zheleznyakov, 1970; see Ginzburg, 1961, 1967; Kakinuma and Swarup, 1962; Krüger, 1979 for more generalized and more complicated formulae):

$$\tau_G = \frac{\pi \nu_p^2 L_H}{c} \left(\frac{v_{th}}{c}\right)^{2n-2} \frac{n^{2n}}{n^{n+1}\, n!} (1 \pm \cos\theta)^2 \sin^{2n-2}\theta$$

$$\approx 1.68 \times 10^{-12} N_e L_H (0.0344)^{2n-2} \frac{n^{2n}}{n^{n+1}\, n!} (1 \pm \cos\theta)^2 \sin^{2n-2}\theta \; . \qquad (2)$$

Here the numerical expressions have been computed assuming an observing frequency of $\nu = 5 \times 10^9$ Hz, an electron temperature of $T_e = 2.5 \times 10^6$ K, an emission measure $\int N_e^2 \, d\ell$ in units of cm^{-5}, a plasma frequency of $\nu_p = 8.9 \times 10^3 \, N_e^{1/2}$ Hz, an electron density of N_e in units of cm^{-3}, and a thermal velocity of $v_{th} = 6.5 \times 10^5 \, T_e^{1/2}$ cm s^{-1}. The angle θ is the angle between the line of sight and the direction of the magnetic field, the scale length of the magnetic field $L_H = H(dH/dz)^{-1}$ is the characteristic dimension for a change in magnetic field strength H, with height, z, and gryoresonant absorption occurs only when the observing frequency $\nu = n \, \nu_H$, where the harmonic n = 2 or 3 in our case and the gyrofrequency $\nu_H = 2.8 \times 10^6$ H cosθ Hz, and the + and - signs respectively refer to the extraordinary and the ordinary modes of wave propagation.

It follows from Equation (1) that the representative optical depths of $\tau = T_B/T_e \approx 0.3$ occur when the emission measure $\int N_e^2 \, d\ell \approx 2 \times 10^{29}$ cm^{-5}, which corresponds to an average electron density $\bar{N}_e \approx 5 \times 10^9$ cm^{-3} when the vertical extent, L, of the radio emitting region is equal to the scale height at 10^6 K ($L = 10^{10}$ cm). The physical parameters inferred under this thermal bremsstrahlung interpretation of the 6 cm radio emission are consistent with those inferred from Skylab X-ray observations of the coronal atmosphere above active regions. The X-rays observations indicate $T_e \approx 2.5 \times 10^6$ K, $\int N_e^2 \, d\ell \approx 2 \times 10^{29}$ cm^{-5}, $L \approx 10^{10}$ cm and $\bar{N}_e \approx 5 \times 10^9$ cm^{-3} for the hot plasma trapped in magnetic arches above active regions (Landini, Fossi, Krieger and Vaiana, 1975; Vaiana, 1976; Vaiana, Krieger, Timothy and Zombeck, 1976; Vaiana and Rosner, 1978). The data given in Section II also indicates that the observed brightness temperature immediately above sunspots can be as low as $T_B < 5 \times 10^4$ K, for which an electron temperature

of $T_e = 2.5 \times 10^6$ K corresponds to an optical depth of $\tau_B < 0.02$; and from Equation (1) an upper limit of $\int N_e^2 \, d\ell < 10^{28}$ cm^{-5} is obtained. This is also consistent with X-ray observations which indicate that the emission measure above sunspots is substantially lower than that above plage with emission measures characteristic of the quiet areas of the solar corona where $\int N_e^2 \, d\ell \sim 10^{27}$ cm^{-5} (Pallavicini, Vaiana, Tofani and Felli, 1979). In summary, then, the interpretation of the enhanced 6 cm emission in terms of the thermal bremsstrahlung of hot, dense "coronal condensations" leads to spatial configurations, emission measures, electron densities, and temperatures which are consistent with those inferred from Skylab X-ray observations of other active regions.

Equation (2) indicates that the gyroresonant absorption layers are transparent for all $n \gtrsim 4$ with $L_H \sim 10^9$ cm and $N_e = 10^9$ to 10^{10} cm^{-3}, whereas the layers are optically thick for $n = 2$ and $n = 3$ at most θ. An optically thin condition can be obtained at $n = 3$ and some values of θ, but hotter brightness temperatures and larger optical depths are expected at larger θ. The observed radiation would therefore be expected to be brightest in regions which are at large angles away from vertical magnetic fields, and this is not generally the case. Moreover, gyroresonant absorption only occurs in a thin layer of thickness $D \lesssim 500$ km, whereas thermal bremsstrahlung occurs throughout the coronal atmosphere. We might therefore imagine that radiation at the second and third harmonic of the gyrofrequency is completely absorbed in a thin layer, but that we actually observe the bremsstrahlung of the hot, dense plasma which is known to overly this layer. Because very special ad hoc assumptions are needed to explain the observed 6 cm radiation in terms of gyromagnetic processes, we prefer the thermal bremsstrahlung process,

especially in view of the fact that the parameters inferred under this assumption are consistent with X-ray observations of other active regions. Nevertheless, we do not want to totally discount the possibility that gyroresonant absorption processes may sometimes play an important role at special wavelengths - particularly when the frequency is at the third harmonic of the gyrofrequency, and in regions near the edges of sunspots where the coronal gas becomes more tenuous and the magnetic field gradients become large. Pallavicini et al. (1979) have, for example, found that intense X-ray sources are always associated with enhanced radiation at 2.8 cm wavelength in regions away from sunspots; and this radio radiation can be accounted for by thermal bremsstrahlung. In some cases, however, they observed enhanced radio emission at 2.8 cm wavelength near sunspots where there is weak X-ray radiation, and this component of radio emission may require the alternative gyroresonant absorption process. Nevertheless, the available data indicate that the thermal bremsstrahlung process plays the dominant role for the plage-associated regions of enhanced emission observed at 6 cm wavelength.

The X-ray data indicate that the topological structure of the coronal magnetic fields largely determines the physical state of the dense coronal plasma, and we see the effects of these intense magnetic fields in the circular polarization of the radio wavelength radiation. When a magnetic field is present, an electromagnetic wave is split into two normal waves, the ordinary, o, and extraordinary, e, waves; and the classical magnetoionic theory can be used to calculate both the optical depths τ_o and τ_e for the two components and the degree of circular polarization, ρ_c, of the emergent radiation. Because linear polarization

has not been detected at 6 cm wavelength, and also because the observed circular polarization shows a strong correlation with the longitudinal magnetic fields seen on magnetograms, we may assume quasi-longitudinal propagation in which (Ratcliffe, 1962; Lang, 1974b, 1980; Krüger, 1979):

$$\tau_o = \frac{\tau}{\left[1 - (\nu_H/\nu)\right]^2}$$

$$\tau_e = \frac{\tau}{\left[1 + (\nu_H/\nu)\right]^2} \qquad (3)$$

and

$$p_c = \frac{\exp(-\tau_e) - \exp(-\tau_o)}{2 - \left[\exp(-\tau_o) + \exp(-\tau_e)\right]} \qquad (4)$$

where τ is the optical depth in the absence of a magnetic field. Optically thick radiation $\tau > 1$ is not polarized even in the presence of a magnetic field. For optically thin bremsstrahlung with $T_B << 1$, Equation (4) becomes:

$$p_c \approx \frac{2\,(\nu_H/\nu)^2}{1 + (\nu_H/\nu)^2} \qquad (5)$$

whereas the optically thin gyroresonant absorption with $T_B << 1$, we have:

$$p_c = \frac{2\cos\theta}{1 + \cos^2\theta} \qquad (6)$$

For both thermal bremsstrahlung and gyroresonant absorption the extraordinary component of wave motion is more strongly absorbed, and the sense

of circular polarization observed at both millimeter and centimeter wavelengths is that of the extraordinary wave. The high degrees of circular polarization observed at centimeter wavelengths require intense magnetic fields if the radiation is bremsstrahlung, for Equation (4) implies magnetic field strengths of H = 450 to 900 Gauss if P_c = 40% to 100% and the optical depth τ = 0.3 to 0.5. This in itself is not a drawback, for the gyroresonant absorption process also requires H = 900 or 600 Gauss because the radiation must be at the second or third harmonic of the gyrofrequency in this case. The gyroresonant absorption does naturally provide high circular polarization for Equation (6) gives $p_c \geq 60\%$ for all θ smaller than seventy degrees, but the optical depths are low at small θ where one observes large circular polarization correlated with longitudinal magnetic fields. The observed circular polarization is not a conclusive test for either radiation mechanism, but it does indicate an optically thin condition in which magnetic field strengths of between 450 and 900 Gauss are required at levels where the temperature exceeds a million degrees.

The observations of solar flares described in the last section showed that the circular polarization decreased as the total intensity of the flare increased. This behavior can be easily understood for if we let $h = (1 + \nu_H/\nu)^2/(1 - \nu_H/\nu)^2$ so that

$$\tau_e = h\tau_o \tag{7}$$

then

$$p_c = \frac{\exp(-h\tau_o) - \exp(-\tau_o)}{2 - \left[\exp(-h\tau_o) + \exp(-\tau_o)\right]} \tag{8}$$

As the burst evolves and the intensity increases, the optical depth will reach its maximum value and the degree of circular polarization will be observed to decrease. The flares that were described in the last section all follow this pattern. Of particular interest is the reversal in sign of the polarization during the flare on December 8 (Figure 19). In order to explain this reversal, it is necessary to consider the effect of a layer of plasma which lies between the source and the observer and which absorbs the emission of the source. If we denote the optical depths in this layer in the extraordinary and ordinary modes by τ_e' and τ_e', then it is easy to show that the degree of circular polarization becomes

$$p_c = \frac{\left[1-\exp(-h\tau_o)\right] - \left\{\left[1-\exp(-\tau_o)\right]\exp(h'-1)\tau_o\right\}}{\left[1-\exp(-h\tau_o)\right] + \left\{\left[1-\exp(-\tau_o)\right]\exp(h'-1)\tau_o\right\}} \qquad (9)$$

where, analagous to equation 7, h' is the factor which relates τ_o' and τ_e' in this layer. If we assume that the observed emission is at the second or third harmonic of the gyrofrequency, the h = 9 or 4, respectively, and in either case the $\exp(-h\tau_o)$ term in equation 9 can be neglected. We then have

$$p_c = \frac{1 - \left[1-\exp(-\tau_o)\right]\exp\left[(h'-1)\tau_o\right]}{1 + \left[1-\exp(-\tau_o)\right]\exp\left[(h'-1)\tau_o\right]} \qquad (10)$$

The value of τ_o' for which the polarization changes sign is thus given by

$$\tau_o' = \frac{-\ell n\ [1-\exp(-\tau_o)]}{h' - 1} \qquad (11)$$

It follows from equation 10 that if the factor $(h'-1)\tau_o'$ decreases during the burst, then the polarization can change sign. If it is assumed that the absorption in the overlying layer is due to the bremsstrahlung process, then from equation 1 it follows that the optical depth will decrease at $T^{-3/2}$, if T, the temperature within the layer increases. If the underlying flare is sufficiently strong, as was apparently the case only for the December 8 burst, then the absorbing layer can be sufficiently heated to cause the opacity to fall below the critical value (11). It has of course been widely discussed in the literature that coronal heating, either prior to and or during a flare, is an essential part of the flare process.

D. CONCLUSIONS

We have presented V.L.A. synthesis maps at 6 cm wavelength for six different active regions on seven different days scattered over a one and a half year period; and we have compared these maps with Hα photographs and magnetograms of the same regions. These pioneering observations and comparisons have allowed us to make some important general conclusions in spite of the fact that the entire V.L.A. was not yet operational. We have shown that the enhanced 6 cm emission of six different active regions comes from one or more small ($\gtrsim$ 20"), bright ($\gtrsim 10^6$K), highly circularly polarized (30% to 100%) sources which are well correlated with the chromospheric plage seen as bright regions on Hα photographs, and that there is often no similar enhanced 6 cm emission in the regions which directly overlay sunspots. We have interpreted the enhanced 6 cm emission in terms of the thermal bremsstrahlung of hot, dense "coronal condensations;" and this interpretation leads to spatial configurations, emission measures $\int N_e^2 d\ell \gtrsim 2 \times 10^{29}$ cm^{-5}, electron densities $N_e \gtrsim 5 \times 10^9$ cm^{-3}, and electron temperatures T_e = 2 to 4 x 10^6 K which are consistent with those inferred from X-ray observations of the coronal atmosphere above other active regions. Our observations are also consistent with X-ray and E.U.V. observations which indicate that a hot, dense plasma is located in magnetic arches between sunspots, and that cooler, tenuous regions overlay sunspots. Our observations also indicate that the circular polarization at 6 cm wavelength exhibits magnetic polarities, dipole shapes, orientations and extents which are correlated with the structure of the longitudinal magnetic field seen in magnetograms of the lower lying photosphere. This indicates that the 6 cm maps of circular polarization delineate the magnetic structure in the solar corona; whereas the high degree of circular polarization can only be explained if the magnetic field strengths lie between 450 and 900 gauss

at coronal levels where the temperature exceeds a million degrees.

Our comparatively large sample suggests some new interpretations of the old (Kundu, 1959a,b) core-halo model in which intense polarized cores (~ 2' in extent) are associated with sunspots, and weak, extended (5' to 9') unpolarized halos are associated with plage. We have found that at 6 cm wavelength the previously unresolved cores are composed of small, bright plage-associated sources which are not necessarily related to sunspots; and that the enhanced 6 cm emission can be explained in terms of the thermal bremsstrahlung of compact "coronal condensations." Because the V.L.A. undersamples the larger angular structures ~ 2', we can say little about the weak and extended halos; but the observations presented here suggest a new multiple component model in which the slowly varying radiation is predominantly due to the thermal bremsstrahlung of a variety of sources ranging from small, dense bright ones to extended, tenuous, dim ones. The increased size of the larger sources might make up for the decrease in brightness, resulting in comparable flux densities from all of the sources. Our multiple component model does not exclude the possibility of important gyroresonant absorption processes in the vicinity of sunspots; but we point out that they require very special conditions in which the observing frequency is at the third harmonic of the gyrofrequency, and that they certainly do not dominate the 6 cm emission from the active regions we have observed. Moreover, because of the confusion and dilution effects of the large antenna beamwidths which included groups of sunspots and bright plage, previously observed intensity and polarization spectra can no longer be used in support of the various models of active regions; and these spectra will have to be redetermined from simultaneous multiple wavelength observations with second-of-arc angular resolution.

We have also presented observations of solar flares at 2.8 cm wavelength using the Owens Valley two-element interferometer. These observations showed that rapid changes in the circular polarization did not occur before the weak to moderate (1 to 10sfu) events that were detected. In a few cases, gradual polarization changes of about 40 percent over a period of about an hour were seen. The strongest flare exhibited changes in both senses of polarization both before and after the impulsive phase of the burst. This is in contrast to the behavior found by Kundu and Vlahos (1979) who observed that bursts of similiar intensity were polarized in only one sense of polarization and only in the impulsive phase. The kind of polarization change observed by us suggests that if the burst arises in a bipolar loop structure, then it comes from opposite magnetic polarities of the loop.

Although our results show that there were no clear pre-flare circular polarization signatures, we feel that further observations during a time when the sun is more active would be useful in order to determine if there is a limit below which bursts of a certain intensity fail to show such "precursors". Observations of flares with the VLA instrument would be of even nore utility as they would be able to provide the positions, sizes, brightness and polarization structures of the bursts with arc-second resolution.

We warmly thank Dr. Don Neidig of the Sacramento Peak Observatory who has sometimes supported our program with simultaneous observations. We are equally grateful to William Livingston of the Kitt Peak National Observatory for providing us with magnetograms, and Viola Miller of the National Geophysical and Solar-Terrestrial Data Center, N.O.A.A., for providing us with the Hα photographs taken with the U.S. Air Force SOON system. We thank Larry R. D'Addario, Barry Clark, Peter Neiper and other members of the V.L.A. staff for their cordial help.

F. REFERENCES

Alissandrakis, C.E. : 1977,Ph.D thesis, Department of Physics and Astronomy, University of Maryland, College Park, Maryland.

Alissandrakis, C.E. and Kundu, M.E. : 1979, Astrophys. J.,222, 342.

Bracewell, R. N.: 1959, Paris Symposium on Radio Astronomy, Stanford University Press, Stanford.

Chiuderi Drago, F., Felli, M., and Tofani, G.: 1977, Astron. Astrophys. 61, 79.

Chiuderi Drago, F., Fürst, E., Hirth, W., and Lantos, P.: 1975, Astron. Astrophys. 39, 429.

Christiansen, W. N. and Mathewson, D. S.: 159, "The Origin of the Slowly Varying Component" in Bracewell (1959) pp. 108-117.

Christiansen, W. N., Mathewson, D. S., Pawsey, J. L., Smerd, S. F., Boischot, A., Denisse, J. F., Simon, P., Kakinuma, T., Dodson-Prince, H., and Firor, J.: 1960, Ann. Astrophys. 23, 75.

Covington, A. E.: 1949, Proc. Inst. Rad. Eng. 37, 407.

Denisse, J. F.: 1950, Ann. Astrophys. 13, 181.

Felli, M., Lang, K. R., and Willson, R. F.: 1980, "V.L.A. Observations of Solar Active Regions I. The Slowly Varying Component" submitted to Astrophys. J.

Felli, M., Pampaloni, P., and Tofani, G.: 1974, Solar Phys. 37, 395.

Felli, M., Poletto, G., and Tofani, G.: 1977, Solar Phys. 51, 65.

Felli, M., Tofani, G., Fürst, E., and Hirth, W.: 1975, Solar Phys. 42, 377.

Foukal, P. V.: 1975, Solar Phys. 43, 327.

Foukal, P. V.: 1976, Astrophys. J. 210, 575.

Friedman, H.: 1961, "X-ray and Extreme Ultraviolet Observations of the Sun" in Space Research II. (ed. H. C. van de Hulst, C. de Jager and A. F. Moore) North Holland, Amsterdam. Reproduced in Lang and Gingerich (1979).

Gelfreich, G., Korol'kov, D., Rishkov, N., and Soboleva, N.: 1959, "On the Regions over Sunspots as Studied by Polarization Observations on Centimeter Wavelengths" in Bracewell (1959) pp. 125-128.

Ginzburg, V.L.: 1961, Propagation of Electromagnetic Waves in Plasma, Gordon and Breach, New York.

Ginzburg, V. L.: 1967, Propagation of Electromagnetic Waves in Plasma, 2nd. Ed., Gordon and Breach, New York.

Ginzburg, V. L. and Zheleznyakov, V. V.: 1959, Sov. Astron. A.J. 3, 325.

Kakinuma, T. and Swarup, G.: 1962, Astrophys. J. 136, 975.

Krüger, A.: 1979, Introduction to Solar Radio Astronomy and Radio Physics, D. Reidel, Boston.

Kundu, M. R.: 1959a, Ann. Astrophys. 22, 1.

Kundu, M. R.: 1959b, "Etude Interferometrique des Sources d'Activite Solaire sur 3 cm de Longueur d'Onde" in Bracewell (1959) pp. 222-236.

Kundu, M.R. and Alissandrakis, C.E.: 1975, Nature 257, 465.

Kundu, M. R., Alissandrakis, C. E., Bregman, J. D., and Hin, A. C.: 1977, Astrophys. J. 213, 278.

Kundu, M. R., Becker, R. H., and Velusamy, T.: 1974, Solar Phys. 34, 185.

Kundu, M. R. and McCullough, T. P.: 1972, Solar Phys. 24, 133.

Kundu, M.R. and Vlahos, L. : 1979, Astrophys. J. 232, 395.

Landini, M., Monsignori Fossi, B. C., Krieger, A., and Vaiana, G. S.: 1975, Solar Phys. 44, 69.

Lang, K. R.: 1974a, Solar Phys. 36, 351.

Lang, K. R.: 1974b, Astrophysical Formulae, Springer-Verlag, Heidleberg

Lang, K.R. : 1977, Solar Physics, 52, 63.

Lang, K. R.: 1980, Astrophysical Formulae 2nd Ed., Springer-Verlag, New York.

Lang, K. R. and Gingerich, O.: 1979, A Source Book in Astronomy and Astrophysics 1900-1975, Harvard University Press, Cambridge, MA.

Lang, K. R. and Willson, R. F.: 1979, Nature 278, 24.

Lang, K. R. and Willson, R.F.: 1980, "Very Large Array (V.L.A.) Observations of Solar Active Regions" in Radio Physics of the Sun: Proceedings of I. A. U. Symposium No. 86, D. Reidel, Boston.

Lantos, P.: 1968, Ann. Astrophys. 31, 105.

Lehany, F. J. and Yabsley, D. E.: 1949, Australian J. Sci. Res. A2, 48.

Newkirk, G.: 1961, Astrophys. J. 133, 983.

Pallavicini, R., Vaiana, G. S., Tofani, G., and Felli, M.: 1979, Astrophys. J. 229, 375.

Piddington, J. H. and Minnett, H. C.: 1951, Australian J. Sci. Res. A4, 141.

Ratcliffe, J. A.: 1962, The Magneto-Ionic Theory, Cambridge University Press, Cambridge.

Stepanov, K. N.: 1958, J. Exp. Theor. Phys. U.S.S.R. 35, 283 (English trans. in Sov. Phys. J.E.T.P. 8, 195 (1959)).

Swarup, G., Kakinuma, T., Covington, A. E., Harvey, G. A., Mullaly, R. F., and Rome, J.: 1963, Astrophys, J. 137, 1251.

Tanaka, H. and Steinberg, J. L.: 1964, Ann. Astrophys. 27, 29.

Vaiana, G. S.: 1976, Phil. Trans. Roy. Soc. (London) A281, 365.

Vaiana, G. S., Krieger, A. S., Timothy, A. F., and Zombeck, M.: 1976, Astrophys. Space Sci. 39, 75.

Vaiana, G. S. and Rosner, R.: 1978, Ann. Rev. Astron, Astrophys. 16, 393.

Waldmeier, M.: 1956, Z. Astrophys. 40, 221.

Waldmeier, M. and Müller, H.: 1950, Z. Astrophys. 27, 58.

Zheleznyakov, V. V.: 1962, Sov. Astron. A. J. 6, 3.

Zheleznyakov, V. V.: 1970, Radio Emission of the Sun and Planets, Pergamon Press, New York.

Zlotnik, E. Ya.: 1968a, Sov. Astron. A. J. 12, 245.

Zlotnik, E. Ya.: 1968b, Sov. Astron. A. J. 12, 464.